Environmental Development 55 (2025) 101210

Contents lists available at ScienceDirect

Environmental Development

journal homepage: www.elsevier.com/locate/envdev

Response of the global ITCZ to ENSO and how the ITCZ determined from maximum precipitation compares with the surface tropical wind convergence

Teke S. Ramotubei [a,b,*], Willem A. Landman [b], Mohau J. Mateyisi [a], Shingirai S. Nangombe [c], Asmerom F. Beraki [b,d]

[a] Council for Scientific and Industrial Research (CSIR), Pretoria, South Africa
[b] Department of Geography, Geoinformatics and Meteorology, University of Pretoria (UP), Pretoria, South Africa
[c] Danish Meteorological Institute (DMI), Sankt Kjelds Plads 11, 2100, Copenhagen, Denmark
[d] ClimateSynth Solutions Inc, Toronto, Canada

ARTICLE INFO

Keywords:
Wavelet analysis
Spatial variation
ERA5 reanalysis
Regional ITCZ
Tropical wind convergence

ABSTRACT

Shifts in the position of the intertropical convergence zone (ITCZ) may lead to amplification of climate extremes such as droughts and flooding. Its spatio-temporal variations respond to well-established oscillation processes like the El Niño Southern Oscillation (ENSO). This research establishes the global and regional response of the ITCZ position to ENSO. It also explores the alignment between the ITCZ as determined from two methods: the surface tropical wind convergence, and maximum precipitation. The ERA5 reanalysis data, 1990–2020, are used in this study. Each longitude is scanned for latitude of maximum precipitation, during each El Niño/La Niña/Neutral year, within the 20°N/S latitude range to identify the ITCZ position. An overlay of surface tropical wind convergence and the ITCZ position is employed for comparison of the two methods. The study concludes that the position established by the maximum precipitation aligns with the surface tropical wind convergence over the global oceanic areas. On seasonal average, the La Niña ITCZ position is consistently southward of its El Niño position over Africa and Central Pacific Ocean. Furthermore, the extreme cases of El Niño/La Niña leads to further north/south shifting of the ITCZ position from its normal El Niño/La Niña positions. The continental and Atlantic Ocean ITCZ is more persistent and shows a minimal fluctuation, in comparison to Oceanic ITCZ, during the El Niño/La Niña. Cross-wavelet analysis was explored as an African case study and it shows common high-power features between the Oceanic Niño Index (ONI) and ITCZ signals over a four-year periodicity, mirroring the ENSO periodicity albeit with slowly varying time lag across the years. The cross-correlation of the two signals is strongest in Austral summer (DJF), corresponding to the peak of ENSO. This study contributes to the understanding of the overall description of the global and regional (with Australia and South America as new additions) ITCZ along with its response to the ENSO phases using the latest ERA reanalysis data. The global/regional spatio-temporal ITCZ shifts open an opportunity for improved interpretation of seasonal forecasts of hydroclimatic events, especially under climate change conditions that reflect a possibility of an increase in the frequency of ENSO events in the future.

This article is part of a special issue entitled: Integrated ECEs published in Environmental Development.

* Corresponding author. Council for Scientific and Industrial Research (CSIR), Pretoria, South Africa.
E-mail address: tramotubei@csir.co.za (T.S. Ramotubei).

https://doi.org/10.1016/j.envdev.2025.101210
Received 16 July 2024; Received in revised form 17 March 2025; Accepted 26 March 2025
Available online 27 March 2025
2211-4645/© 2025 The Authors. Published by Elsevier B.V. This is an open access article under the CC BY-NC-ND license (http://creativecommons.org/licenses/by-nc-nd/4.0/).

1. Introduction

The intertropical convergence zone (ITCZ) is currently attracting significant research attention. According to Wolf et al. (2020), more research work directed towards understanding the dynamics of the ITCZ is required. Furthermore, the role of internal variability and external radiative forcing on the spatial position of the ITCZ remains a key open research question. Studies demonstrate that the location of the ITCZ does not only vary according to the input data (Liu et al., 2020) but also methods used (Burns et al., 2022; Lashkari et al., 2017; Mischell and Lee, 2022; Roldán-Gómez et al., 2022; Vindel et al., 2020; Wei and Bordoni, 2020). However, it is important to study the variations and possible drivers of the ITCZ position evolution over different regions. Such studies are valuable in informing a better representation of the ITCZ process within climate models (Wu et al., 2003). To date, climate models are struggling to consistently simulate and project the ITCZ features that are aligned to the overall projections of the future climate according to different emission scenarios (Liu et al., 2020; Wolf et al., 2020). Therefore, a thorough understanding of the spatio-temporal responses of the ITCZ, especially to slow drivers of climate variability, is essential for improving the model representation of the process.

In addition, the improvement is relevant across short range to seasonal time scales (Tadeyo et al., 2020). The variability of the ITCZ position is influenced by a variety of factors including insolation (radiation), convection, and circulation (Burns et al., 2022; Lau et al., 2020; Randriatsara et al., 2022). This variability is not only important as the link to extra-tropical weather systems (Frierson and Hwang, 2012) but also to the livelihoods of the people within the tropics (Liu et al., 2020). Furthermore, ITCZ position shows a spatial variability that aligns with climate drivers such as the distribution of the global oceans and continents (Roldán-Gómez et al., 2022; He et al., 2014; Khan and Arsalan, 2008; Xu et al., 2010). On the African continent, for example, the position of the ITCZ is known to be related to the El Niño Southern Oscillation (ENSO) phases, the North Atlantic Oscillation (NAO), and the local meridional temperature gradient (Liu et al., 2020).

Recent studies explored the spatial variation of the ITCZ by focusing on specific domains of interest; Adam et al. (2016) carried their ITCZ position variability over 0° - 60°E while Suzuki (2011) carried out a related study over 10°E to 40°E. Roldán-Gómez et al. (2022) explored the spatial ITCZ over the Pacific, Atlantic and Indian ocean basins, leaving out the continents in between. Mischell and Lee (2022) explored the spatial variation of the ITCZ over the Indian, Pacific, Atlantic, Western Pacific, Central Pacific, and Eastern Pacific Oceans. The centroid method or the maximum precipitation method are used among all the studies for the quantification of the position of the ITCZ. None of these studies established a link between the estimated ITCZ position and the tropical surface wind convergence patterns. Such a connection has been established by Keshtgar et al. (2020) by exploring the differences between ITCZ position as represented by maximum precipitation to that represented by minimum divergence over the Indian ocean. They concluded that maximum precipitation and minimum divergence yield a similar ITCZ zonal position over the Indian ocean. A global comparison of the positions of the ITCZ identified via maximum precipitation and surface tropical wind convergence, especially during extreme phases of ENSO, is worth undertaking to set the basis for global model evaluation under the climate extremes.

This study investigates the global ITCZ position using the maximum precipitation and surface tropical wind convergence and its response to the ENSO phases. Specifically, the seasonal shifts of the ITCZ position, including extreme ENSO events are analyzed. The seasonal transition of the ITCZ position in response to North vs South differential heating gradients is also discussed relative to the maximum precipitation patterns. The study also explores the co-variability of the seasonal ENSO signal with the seasonal ITCZ over Africa.

2. Data and methodology

2.1. Data selection and acquisition

The global reanalysis dataset from the European Centre for Medium-Range Weather Forecasts (ECMWF) fifth generation reanalysis (ERA5) at 0.25° * 0.25° resolution (Hersbach et al., 2020) is utilized in this study. ERA5 based precipitation is strongly correlated with gridded observational precipitation from Climate Hazards Group Infrared Precipitation with Stations (CHIRPS) and Climate Research Unit (CRU) datasets over different regions of the Globe (Gleixner et al., 2020; Morales-Velázquez et al., 2021; Mosaffa et al., 2023; Navidi Nassaj et al., 2022; Silva et al., 2022; Steinkopf and Engelbrecht, 2022) and a suitable dataset for use in statistical downscaling (Horton, 2022). The study period used (1990–2020) is aligned to the latest climatology period according to the World Meteorological Organization's (WMO's) climate timelines (Arguez and Vose, 2011). This time series is divided into nine El Niño years, three neutral years, and ten La Niña years that are based on the Oceanic Niño Index (ONI). ONI is based on three month running mean of sea surface temperature (SST) anomalies in the Niño 3.4 Ocean region as obtained from the Extended Reconstructed Sea Surface Temperature version5 (ERSSTv5) (Huang et al., 2017). Only the ERA5 dataset is used in this study. This choice is supported by multiple studies (Gbode et al., 2023; Quagraine et al., 2020; Shen et al., 2020; Steinkopf and Engelbrecht, 2022) which confirm that there are minimal differences (in terms of areas of intense precipitation) between the CRU gridded Time Series version 4 (CRU TS v4), the CHIRPS version 2 (CHIRPS2.0) and ERA-based datasets. ERA5 dataset was chosen because it also has the surface wind, and the SST data required for the study.

2.2. Study area

A global domain between 20°N and 20°S was selected for the study to allow for comparison with previous studies. Additionally, sub-regions were selected for a detailed analysis and the respective domains were selected as per literature sources depicted in Table 1.

Table 1
Study regions and their respective longitude ranges.

Region Explored	Longitudes	Following classification by:
Africa	0-60°E	Adam et al. (2016)
Indian Ocean	60°-100°E	Mischell and Lee (2022) and Suzuki (2011)
Australia	100°-155°E	**This article**
Western Pacific (WPacific) Ocean	110°-150°E	Mischell and Lee (2022) and Suzuki (2011)
Central Pacific (CPacific) Ocean	160°E–160°W	
Eastern Pacific (EPacific) Ocean	100°-140°W	
South America (SAmerica)	40°-80°W	**This article**
Atlantic Ocean	10°-40°W	Mischell and Lee (2022)

2.3. Index calculation

Identification of the ITCZ position using seasonal precipitation is achieved by scanning for the latitude (between 20°N/S) of maximum seasonal precipitation along each longitude following a similar approach implemented by Liu et al. (2020); Marshall et al. (2014); Waliser and Gautier (1993). These studies calculated the latitude corresponding to the maximum of the zonally averaged (over the globe or specific region of interest) precipitation for zonal position or the latitude of maximum precipitation along each longitude, confined within the tropics (20°N/S) for spatial position. The latter method was applied to identify the spatial position of the ITCZ while the zonal position was estimated by averaging the identified spatial positions.

Identification of the ITCZ position by surface wind is done by locating the convergence area of the surface trade winds as done in Zhu et al. (2018) and Grodsky (2003). The methods either identified the changing wind direction/strength through low-level wind field anomalies or calculated the zonal wind along each latitude and identified the latitude of the highest wind strength. In this study, an area where the wind changes from the easterlies to westerlies or an area where the north-easterlies meet the south-easterlies is considered to represent the area of convergence. Furthermore, the total horizontal divergence is calculated and the latitude of minimum total horizontal divergence along each longitude is identified.

For the implementation of the total horizontal divergence calculation, the surface (10m) wind data was used. The calculation was done using the meteorological python library for data analysis and visualization (MetPy) software (May et al., 2022) which deploys the following total horizontal divergence formula:

$$\nabla \cdot \vec{U} = \frac{\partial u}{\partial x} + \frac{\partial v}{\partial y},$$

Where u is the zonal wind and v is the meridional wind. This formula considers the changes in wind direction and speed to calculate the total horizonal divergence. Thereafter, each longitude was scanned for the latitude of minimum divergence (Min_Div) within the tropics (20°N/S) following a similar approach to one applied in identifying the ITCZ position using maximum precipitation.

2.4. Data analysis

Global sea surface temperature (SST) patterns influence the spatio-temporal dynamics of the ITCZ (Mischell and Lee, 2022; Wolf et al., 2020). Therefore, the seasonal position of the ITCZ which is an area of intense precipitation (Philander et al., 1996; Roldán-Gómez et al., 2022) and maximum surface wind convergence (Faulk et al., 2017) is plotted with an overlay of.

i. Surface total divergence to portray areas of minimum divergence (maximum convergence),
ii. Wind vectors to depict areas where wind changes from easterlies to westerlies or south-easterlies meet the north-easterlies,
iii. Seasonal SSTs for visual analysis of their influence on the spatio-temporal variation of the ITCZ.

The wavelet analysis of the 1950–2022 ONI is done to determine the periodicity of the ENSO events and the associated variance within the 2–8 years averaged power. The goal is to identify the periodicity of the ENSO events and to study the coherence between the North-South migration of the African ITCZ and the ENSO periodicity. The procedure for generating the wavelet, cross-wavelet, and coherence analysis followed that of Torrence and Compo (1998) and Torrence and Webster (1999). Specifically, the timeseries of the ITCZ position, over Africa, and that of the Niño 3.4 ONI were extracted for cross-wavelet spectrum and coherence analysis. The wavelet, cross-wavelet, and coherence analysis between ONI and ITCZ signals for each of the four rolling Austral summer seasons was done for the period 1990–2020. This made an analysis of the association between ENSO phases and the ITCZ in both time and frequency space possible. Spatial standard deviation (σ) is calculated for regions in Table 1 to measure the North/South variability of the ITCZ from its mean spatial position during the ENSO phases.

This study focuses on the period from the beginning of the Austral summer season to the beginning of Austral autumn season, covering the months from November of the current year (t_0) to April the following year (t_0+1). This period was used because it includes the onset and cessation of the southern hemisphere summer precipitation. The El Niño/La Niña year in this context covers from November of year t_0 into April of year t_0+1. Similarly, the NDJ season consists of November and December from year t_0 and January from year t_0+1 while DJF is made up of December from year t_0 with January and February from year t_0 +1. JFM (January to March)

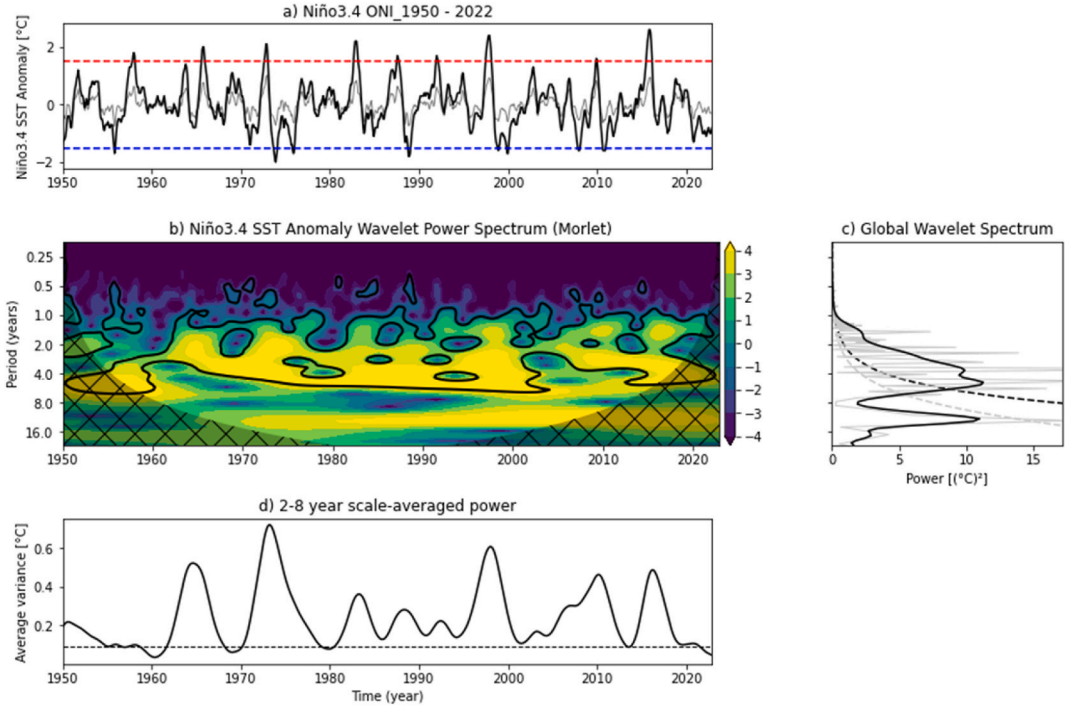

Fig. 1. Wavelet transform of the 1950–2022 seasonal and original Oceanic Niño Index (ONI) time series (a). Normalized wavelet power spectrum of the Niño 3.4 SST anomalies using the Morlet wavelet (b). Global wavelet spectrum (solid black line) and the Fourier power spectrum (solid grey line) with the 5 % significance level (black dotted line) and the red noise (grey dotted line) are presented by (c). The variance in 2–8 years scale-averaged power is presented by (d). (For interpretation of the references to colour in this figure legend, the reader is referred to the Web version of this article.)

and FMA (February to April) are from year t_0+1. A year, as defined, is regarded to be an El Niño/La Niña year provided the phase remains active in three of the four (NDJ, DJF, JFM, and FMA) seasons. Therefore, the active El Niño years between 1990 and 2020 are 1991/92 (from November 1991 to January 1992), 1994/95, 1997/98, 2002/03, 2004/05, 2009/10, 2014/15, 2015/16, and 2018/19 while the active La Niña years are 1995/96, 1998/99, 1999/2000, 2000/01, 2005/06, 2007/08, 2008/09, 2010/11, 2011/12, and 2017/18. The three extreme El Niño years identified between 1990 and 2020 are 1991/92, 1997/98 and 2015/16 while the three extreme La Niña years are 1998/99, 1999/2000 and 2010/11. The extreme El Niño (La Niña) years were identified as those years when the ONI was greater (less) than 1.5 °C (−1.5 °C) as reflected by the red (blue) dotted lines in Fig. 1 (a).

The ONI data used to generate Fig. 1 can be accessed from the National Centers for Environmental Prediction (NCEP) of the National Oceanic and Atmospheric Administration (NOAA) website. Wavelet analysis was applied to the data to identify the ONI periodicity in the long-term time series. The cross hatched area in Fig. 1b represents the cone of influence (COI) where the wavelet power spectra are distorted because of the end points of the finite length signal. The red noise symbolizes an area in which there is an increase in power with increasing frequency.

There is a 95 % confidence (the thick black contours in Fig. 1b) for 2–8 years ENSO periodicity. The Morlet wavelet power spectrum is an accurate estimation of the ONI signal's Fourier power transform (Fig. 1c) which indicates that we can use Morlet wavelet in cross-wavelet and cross-correlation analysis between the ONI and ITCZ position. According to Fig. 1d, the ONI had a high variance between 1960s to around 1975 from which it had a downward trend into the late 1990s. The variance reflects an increasing trend again from the 2000s until around the 2020s. Therefore, this research explores the relationship between ITCZ and the ONI during the period of relatively more active ENSO.

3. Results and discussion

One of the key questions investigated in this study is whether the ITCZ, as determined by maximum precipitation, aligns with the convergence of the surface tropical winds. This is addressed in subsection 3.1. In the subsequent subsection, the impact of ENSO phases on the ITCZ positioning is interrogated. Specifically, whether the ITCZ shifts North/South during El Niño (La Niña) and the impacts of extreme El Niño (extreme La Niña) on this shift are discussed (subsection 3.2). Finally, the results cover a question on how the ITCZ position relates to the actual seasonal SSTs during the different ENSO phases (subsection 3.3). This final subsection includes an African case study on the application of the seasonal wavelet transform and coherence analysis to identify the periodicity of the ENSO phases, and the coherence between the seasonal ONI and the seasonal ITCZ. To summarize, the spatial standard deviation is used to measure the level of variability in the spatial ITCZ over different regions as outlined in Table 1.

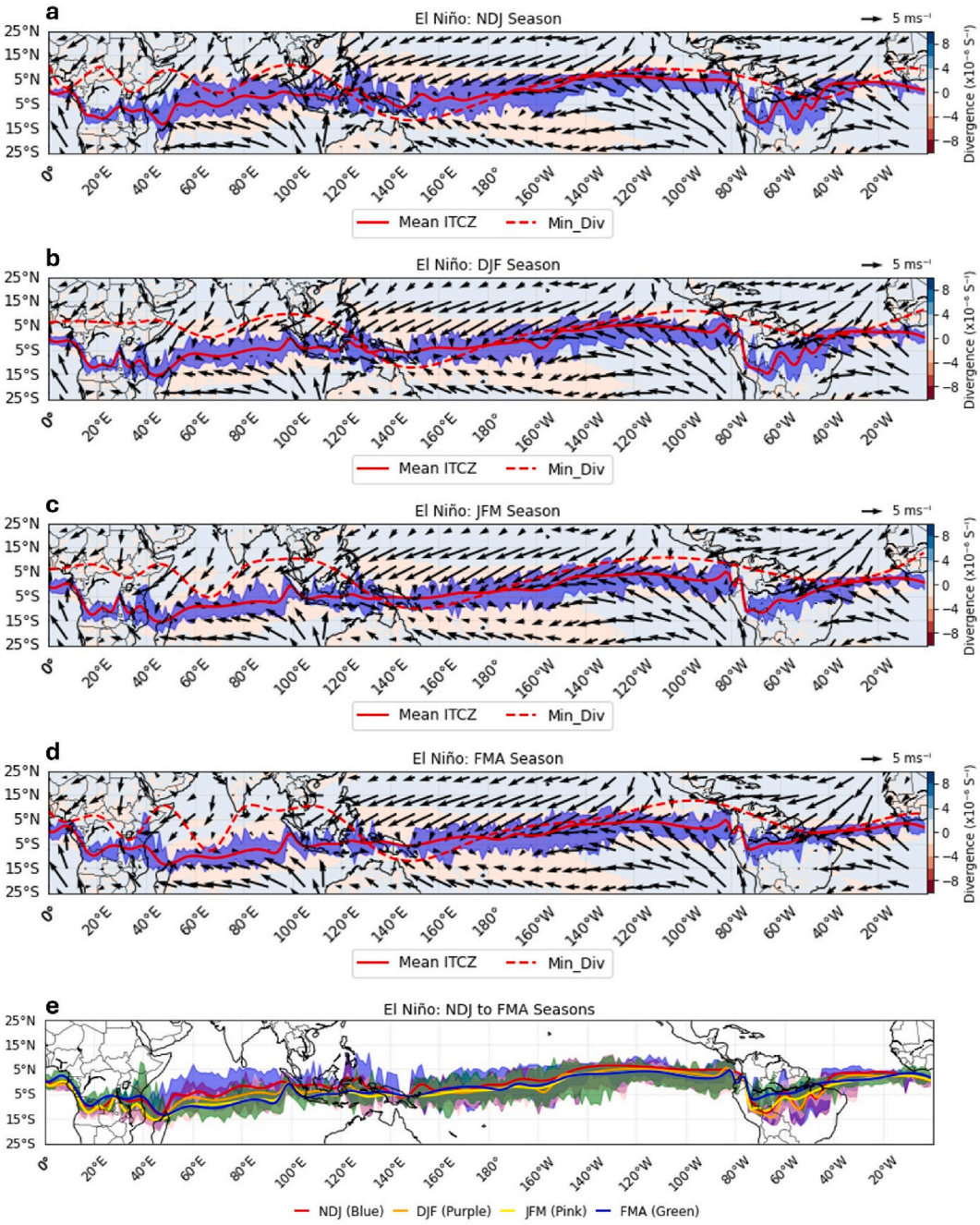

Fig. 2. Seasonal mean ITCZ position determined from maximum precipitation (red solid line with blue plume, for year-on-year variability, around it) and surface minimum divergence (Min_Div, red dotted line) overlaid on seasonal surface (10m) tropical wind and seasonal divergence (x10^{-6}s^{-1}) during the El Niño phase for NDJ (a), DJF (b), JFM (c), and FMA (d) seasons. A comparison of the spatio-temporal variation of the seasonal ITCZ is presented by (e). The plume colour for each season is shown in brackets. (For interpretation of the references to colour in this figure legend, the reader is referred to the Web version of this article.)

3.1. Maximum precipitation derived ITCZ compared with the surface wind convergence

3.1.1. El Niño

The surface tropical wind convergence over the Indian Ocean, WPacific Ocean, EPacific Ocean, and Atlantic Ocean are well aligned to the position of the ITCZ during El Niño. The only oceanic area that shows complexity and limited alignment to the line of wind convergence, is the CPacific Ocean. This is also the region where double ITCZ exists (Chen et al., 2021; Liu et al., 2020; Yan and Li,

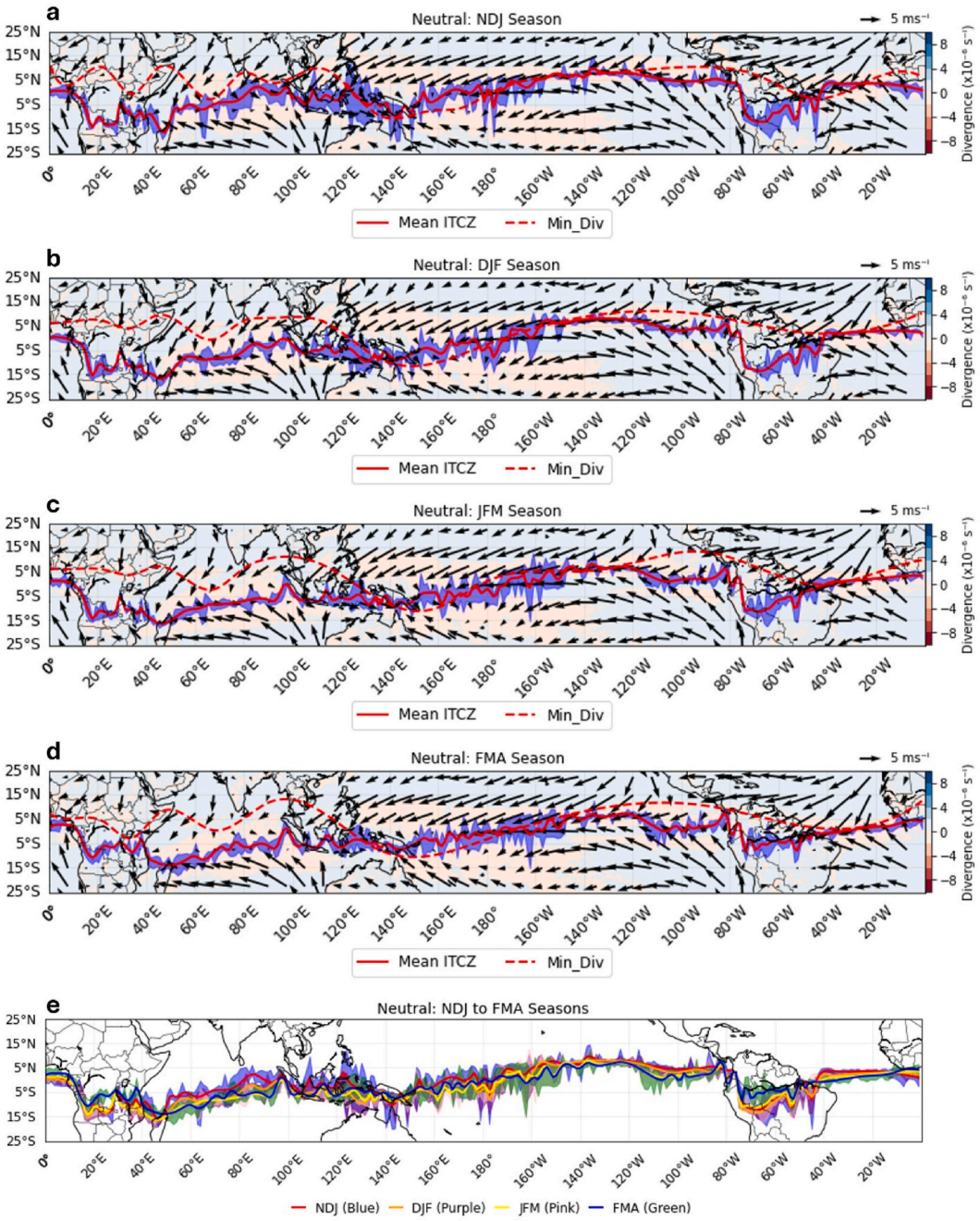

Fig. 3. ITCZ position determined from maximum precipitation (red solid line with blue plume around it) and minimum divergence (Min_Div, red dotted line) overlaid on seasonal surface (10m) tropical wind and seasonal horizontal divergence ($x10^{-6}s^{-1}$) during the Neutral phase for NDJ (a), DJF (b), JFM (c), and FMA (d). Variation of the ITCZ from NDJ to FMA together with their year-on-year variation per season (plume colour in brackets for each season) is presented by (e). (For interpretation of the references to colour in this figure legend, the reader is referred to the Web version of this article.)

2018). Interestingly, the seasonal surface wind over CPacific shows a large area (corresponding to dual ITCZ region) of no clear wind directions and speeds. However, the seasonal ITCZ mean position is found within the southern and northern bounds of the north-easterly and south-easterly winds, respectively. The minimum divergence line is also found within the bounds of the north-easterly and south-easterly winds. The shaded minimum horizonal divergence on the background shows the distribution that coincides with areas of high precipitation values corresponding to the dual ITCZ. There is no alignment between the ITCZ and the surface tropical wind convergence over the continents. The interannual variation of the ITCZ has a higher propensity for a more northerly shift over the Indian ocean through to the Western Pacific in NDJ (blue plume) while there is a higher inclination for a

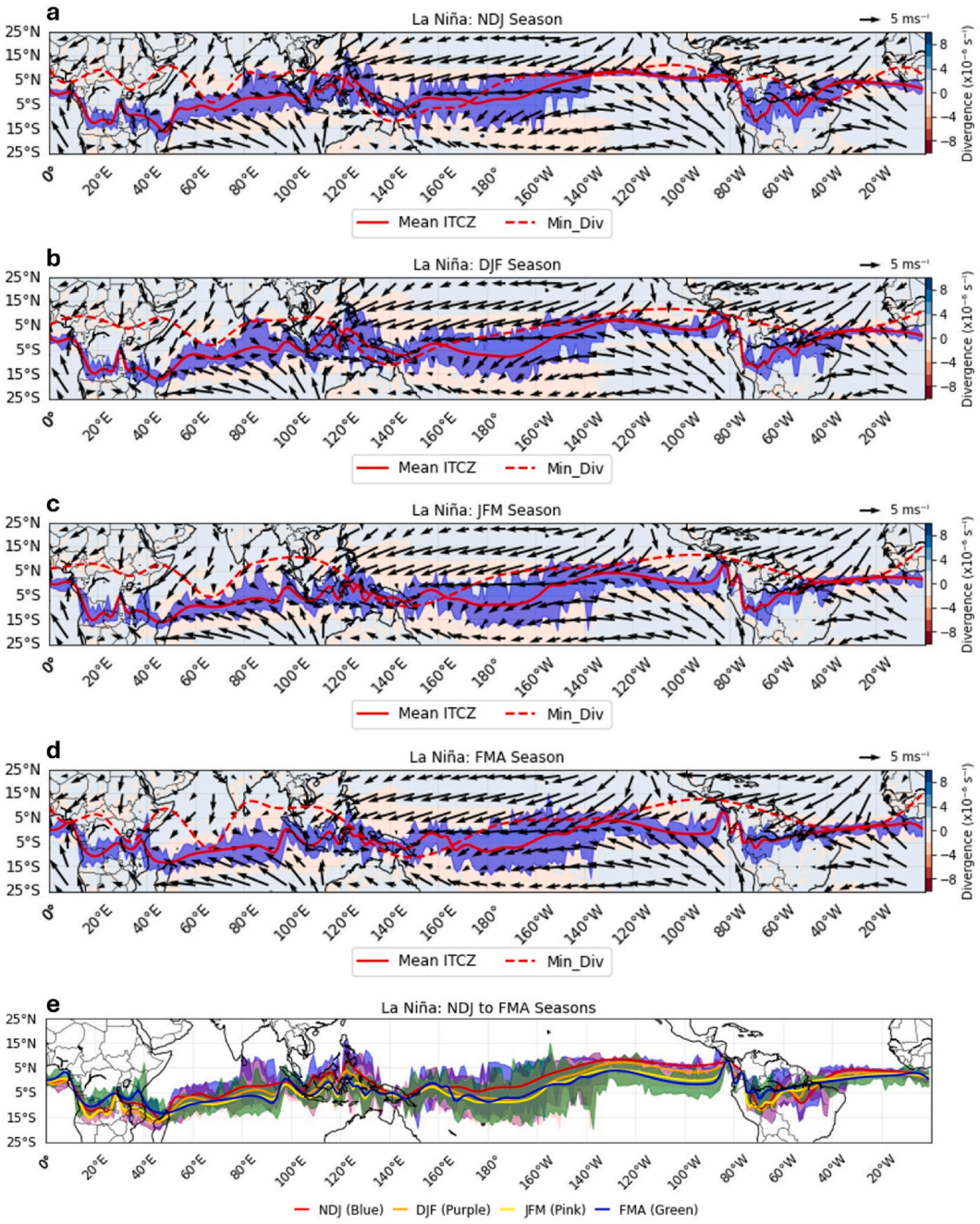

Fig. 4. ITCZ position determined from maximum precipitation (red solid line with blue plume around it) and minimum divergence (Min_Div, red dotted line) overlaid on seasonal surface (10m) tropical wind and seasonal horizontal divergence ($x10^{-6}s^{-1}$) during the La Niña phase for NDJ (a), DJF (b), JFM (c), and FMA (d). Lastly, (e) shows the NDJ, DJF, JFM, and FMA position with their respective plume colour in brackets. (For interpretation of the references to colour in this figure legend, the reader is referred to the Web version of this article.)

southerly shift over South America in DJF (purple plume) and JFM (pink plume) during El Niño phase (Fig. 2e).

3.1.2. Neutral

The surface tropical wind convergence over the oceans (except the CPacific to WPacific oceans) is well aligned to the ITCZ position for all seasons during the neutral phase of ENSO (Fig. 3a–d). There is no propensity for a consistent northerly or southerly shift of the spatio-temporal ITCZ from NDJ to FMA during the neutral ENSO. Rather, ITCZ shows a frequent north-south fluctuation within the short east-west angular distances. Furthermore, the plume showing year-on-year variation does not cover the area between the north-

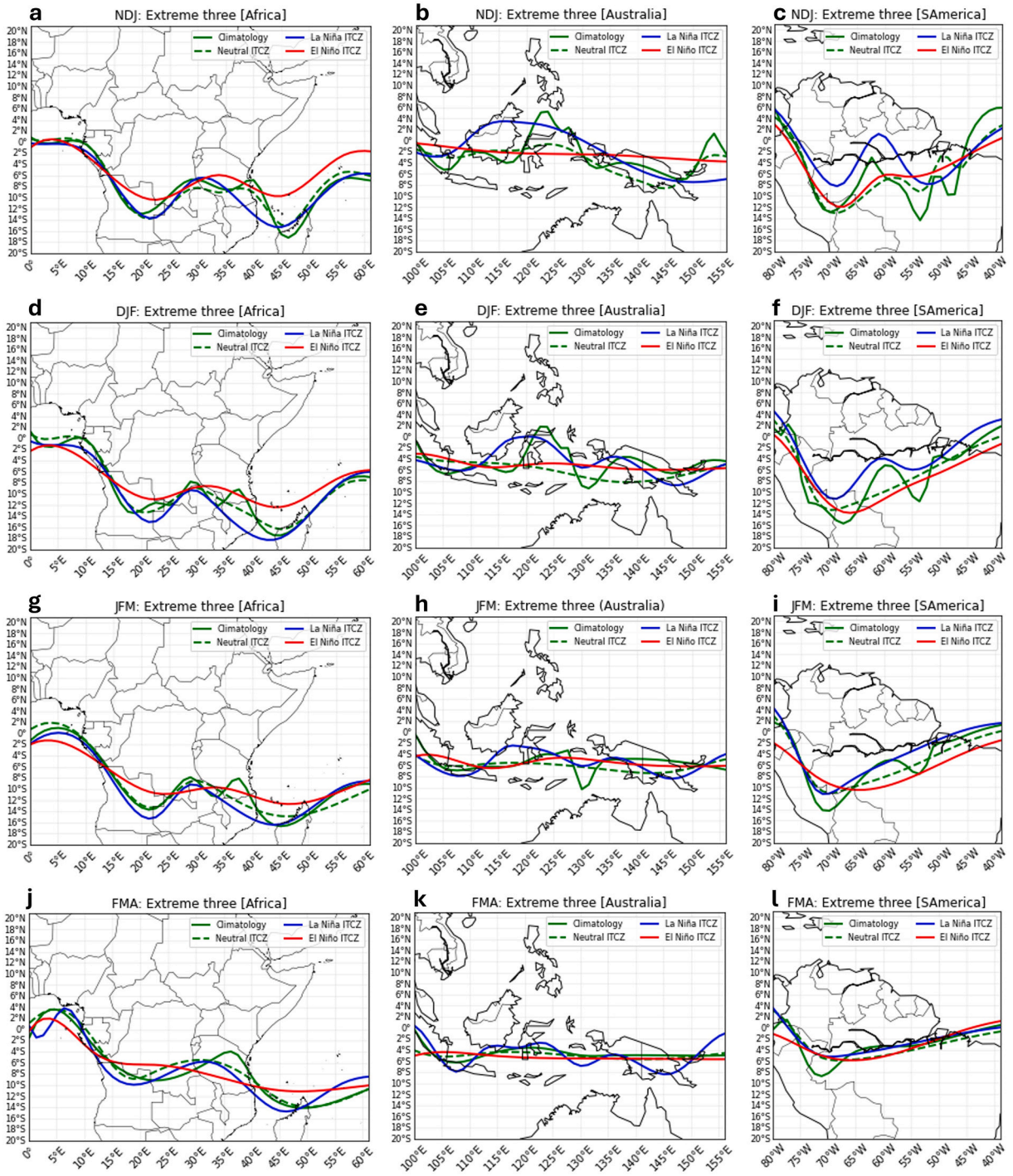

Fig. 5. Continental comparison of the spatial ITCZ position between the extreme El Niño, extreme La Niña, and Neutral phases of ENSO and the Climatology for NDJ, DJF, JFM & FMA seasons between 1990 and 2020. The three continents are Africa (0°-60°E), Australia (100°-155°E), and South America (40°-80°W) with seasons respectively represented by a-c (NDJ), d-f (DJF), g-i (JFM), and j-l (FMA).

easterly and south-easterly winds over the CPacific and WPacific Oceans. The frequent north-south ITCZ fluctuation within short east-west angular distance is consistent with what is discussed in section 3.3 where it is found that the neutral ENSO and climatological ITCZ display higher spatio-temporal variability than the El Niño/La Niña phases of ENSO. Similarly, there is no alignment between the maximum precipitation-based and surface tropical wind convergence-based positions of the ITCZ over the continents. The variation of the ITCZ has a higher tendency towards a more northerly shift over the Indian ocean through to the Western Pacific during NDJ (blue

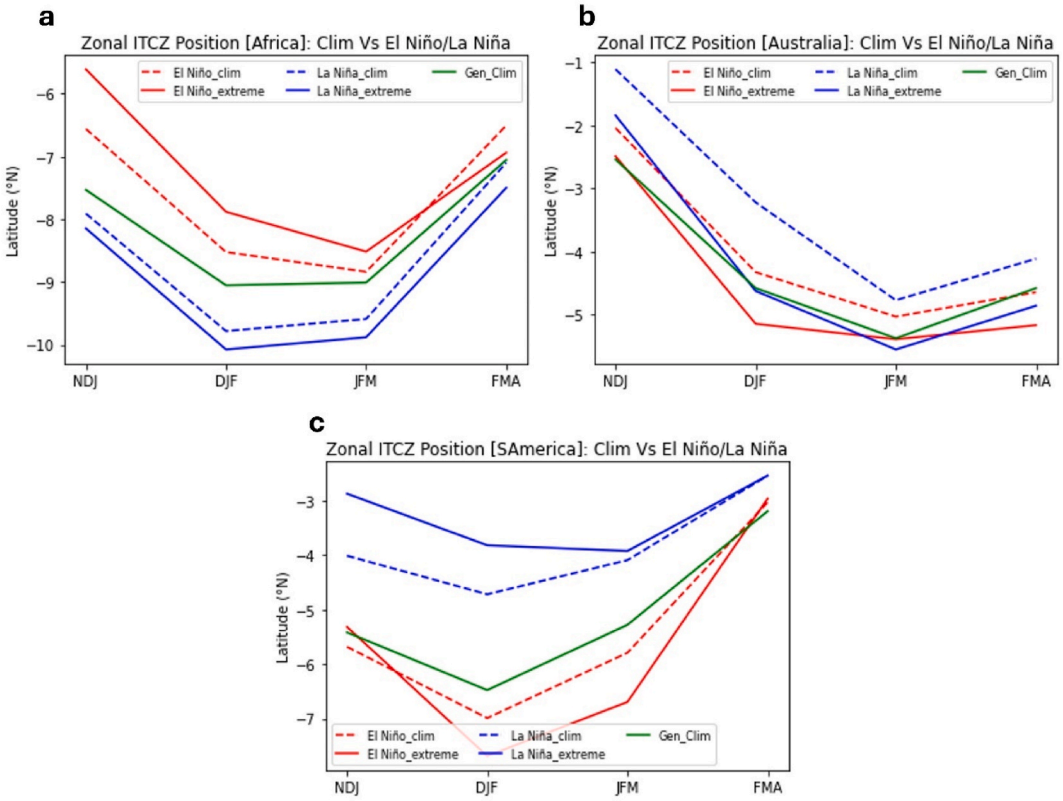

Fig. 6. Comparison of the continental and zonal ITCZ position during extreme El Niño, extreme La Niña, and Neutral phases of ENSO and the Climatology for NDJ, DJF, JFM & FMA seasons. The three continents are Africa (a), Australia (b), and South America (c) with Longitudes 0–60°E, 100–155°E, and 40–80°W respectively.

plume) while there is a proclivity for a higher southerly shift over Australia and South America during the DJF (purple plume) and JFM (pink plume) of the neutral ENSO seasons (Fig. 3 (e)).

3.1.3. La Niña

The surface tropical wind convergence over the Oceans (except the CPacific and WPacific) are well aligned to the position of the ITCZ for all seasons during La Niña (Fig. 4a–d). However, even though there is no alignment over the WPacific and the CPacific, the plume covers the entire area between the north-easterly wind and the south-easterly wind. This shows, in consideration of the existence of double ITCZ over this region (Samanta et al., 2019), that the position of the ITCZ occurs within the possible convergence area. In comparison, the alignment of maximum precipitation and surface wind convergence over the Atlantic Ocean is the closest throughout all the seasons. There is still no sign of alignment over the continental areas. The ITCZ does not show a clear tendency for a northerly or southerly shift in any season, except during DJF and JFM over South America in negative ENSO (La Niña) years (Fig. 4e).

In general, the ITCZ position as determined by maximum precipitation coincides with the surface tropical wind convergence (line or area of convergence) over the oceans (with slight complexity over the areas in which double ITCZ is found) during the El Niño/La Niña. According to Gonzalez et al. (2022), NDJ surface tropical wind convergence over the Pacific Ocean reflect the existence of the double convergence zones. The overlain wind barbs in NDJ season during the three ENSO phases, Figs. 2–4 (a), are aligned to the overlain wind vectors in Fig. 2 from Gonzalez et al. (2022). There are also noticeable differences between the ITCZ position as determined by maximum precipitation and the surface tropical wind convergence, especially over the central to western Pacific Ocean during all the three phases of ENSO and all seasons. Furthermore, the surface tropical line-convergence of wind is not well demarcated over the CPacific and WPacific Oceans (except during the extreme El Niño), possibly owing to the double ITCZ (and its collapse to a more equatorial ITCZ during extreme El Niño, fully addressed in section 3.2).

The alignment of surface tropical winds over the Indian, EPacific, and Atlantic oceans found here aligns with the findings of Gonzalez et al. (2022) that a strong correlation exists between surface convergence and precipitation rate over the east Pacific and Atlantic oceans. Gonzalez et al. (2022) used ERA5 10m horizontal wind and tropical rain measuring mission (TRMM) precipitation datasets in their study. The study by Keshtgar et al. (2020) found that the zonally averaged maximum precipitation is strongly correlated (correlation coefficient of 0.7 at 95 % confidence level) to the zonally averaged minimum divergence over the Indian Ocean (40° - 110°E) for DJF season climatology. This is what we have also found (Appendix G (b)) even with slightly different longitudinal dimensions of the Indian Ocean (60°E – 100°E in this study). Our result is, again, similar to the recent Windmiller and Stevens (2023)

Table 2
NDJ Spatial std deviation (°N/S).

Region	El Niño	Neutral	La Niña	Climate
Africa	4.07	5.16	5.05	5.13
Indian	1.95	3.18	3.38	3.22
Australia	2.09	3.24	4.60	3.86
WPacific	2.08	3.37	4.55	3.86
CPacific	1.59	3.10	4.23	2.03
EPacific	1.28	1.74	0.91	0.80
SAmerica	4.96	5.61	4.85	6.81
Atlantic	1.54	0.32	1.17	0.58

in that the maximum precipitation (in July and August) over the Atlantic ocean is closely aligned to the wind confluence determined using a combination of ERA5 datasets and the data collected through the German research Vessel (SONNE).

The zonal maximum precipitation colocation with the zonal minimum horizontal divergence gets more complex during the different ENSO phases. According to Figs. 2–4, the minimum horizontal divergence consistently occurs to the north of the maximum precipitation for the Austral summer seasons during the different ENSO phases. This is comparable to the climatological findings by Keshtgar et al. (2020) that the energy flux equator (EFE) is always located to the north of the maximum precipitation.

As seen in Figs. 2–4 and Appendix G, surface wind direction and minimum of total horizontal divergence are not well defined over the continents. Therefore, it is not advisable to identify the position of the ITCZ using the wind direction and minimum of total horizontal divergence of surface tropical wind over the continents. This is an observation that also aligns with Nicholson (2018). This result could be associated with the fact that summer maximum precipitation is mostly a result of heat driven convergence (more transient forcing), over the continents than the more resilient large scale global circulation winds.

3.2. Global ITCZ climatology compared with extreme El Niño/La Niña and neutral phases

The neutral and extreme El Niño/La Niña phases are represented by the average of the three neutral years and the average of the three extreme El Niño/La Niña years to investigate the response of the ITCZ to the extremes of ENSO. The average of the three neutral years is used for consistency in comparisons between the extremes of ENSO and the neutral phase.

Fig. 5(a–l) explores the possible existence of significant differences in the ITCZ position during the three different ENSO phases and the climatological ITCZ position during each Austral summer season over the continental areas. The oceanic areas are presented by Appendix B – E for NDJ, DJF, JFM, and FMA respectively. The climatological shift (from around 10°S to around 10°N) of the ITCZ position within the proximity of 160°W (Appendix B (d)) is in response to a shift resulting from the existing two areas of maximum precipitation north and south of the equator known as the double ITCZ (Chen et al., 2021; Zhang et al., 2021). The visualized spatial ITCZ over the continents (Fig. 5(a–l)) and the Atlantic Ocean (Appendix B-E (d)) shows minor (greater) differences between the climatology and neutral (El Niño and La Niña) ENSO phase for all the seasons (NDJ, DJF, JFM & FMA), also reflected in Appendix A (Tables 6 and 7).

The zonal position of the African ITCZ shifts north during El Niño (red dotted line) reaching its northernmost position during the extreme El Niño (red solid line), except for FMA season. Fig. 6a further shows that the African ITCZ shifts southward during La Niña (blue dotted line) reaching its southermost latitude during the extreme La Niña (blue solid line). The SAmerican ITCZ response to the extreme ENSO phases is opposite to the African ITCZ response; the ITCZ shifts south of its climatological position during El Niño while it shifts north of the climatological position during La Niña (Fig. 6c). This is aligned to the general response of the tropical precipitation over South America during El Niño/La Niña (Lenssen et al., 2020) with the extremes only enhancing this response. The Australian zonal ITCZ remains north of the climatological position during both El Niño and La Niña phases. However, it shifts south of the climatological position during the extremes (Fig. 6b). Notwithstanding, the ITCZ position during extreme La Niña over Australia is comparable to the normal El Niño and climatological positions. The ITCZ over EPacific (Appendix F (c)) and Atlantic Ocean (Appendix F (d)) remains to the south of its climatological position during El Niño, La Niña and their extremes.

The response of the ITCZ position over the Indian Ocean (Appendix F (a)), and CPacific (Appendix F (b)) Oceans remain unique from all the other regions. Interestingly, there exists a minimum difference and overlaps (from DJF season to the JFM season) between the climatological position and the El Niño/La Niña positions over the Indian Ocean. The ITCZ over the WPacific is not shown because it is similar to the Australian ITCZ. The extreme El Niño case over the CPacific is bound by the climatological and normal El Niño positions of the ITCZ, except during NDJ where the position during extreme El Niño occurs south of both the climatological & normal El Niño positions.

Comparing the climatological position to the neutral ENSO phase, the largest difference (in magnitude) between the positions is found within the Central (with a difference of ≅ 4°) and Western Pacific (with a difference of 1.14°) Oceans. Furthermore, the position of the ITCZ during the neutral phase remains to the north of the climatological position except over Australia, WPacific, SAmerica, and Atlantic Ocean. It is worth noting, however, that the positional difference between the climatological and neutral ENSO remains, at most, 1° except for the Central Pacific. This reflects the sensitivity of the seasonal precipitation distribution to the SST changes (ENSO phases) over the CPacific Ocean. Comparing the extreme El Niño, extreme La Niña and climatology position of the ITCZ from November–April, leads to a conclusion that the extreme ENSO cases collapse the double-ITCZ to a single and more equatorial ITCZ. This is seen by the absence of an abrupt shift, as shown by the El Niño/La Niña climatological position, from the southern ITCZ to the

Table 3
DJF Spatial std deviation (°N/S).

Region	El Niño	Neutral	La Niña	Climate
Africa	4.00	5.66	5.88	5.62
Indian	1.76	3.13	3.14	3.14
Australia	1.93	2.29	3.22	3.46
WPacific	2.00	2.34	3.46	3.75
CPacific	1.41	3.10	3.16	1.24
EPacific	1.29	1.97	1.56	1.03
SAmerica	5.29	5.42	5.05	6.54
Atlantic	1.52	0.56	0.55	0.30

Table 4
JFM Spatial std deviation (°N/S).

Region	El Niño	Neutral	La Niña	Climate
Africa	4.43	5.79	5.62	5.58
Indian	2.07	2.68	3.00	3.54
Australia	1.66	1.95	2.74	2.91
WPacific	1.68	1.92	2.87	3.15
CPacific	1.59	3.10	2.02	2.04
EPacific	0.97	2.52	1.93	2.31
SAmerica	4.25	4.61	4.76	5.31
Atlantic	1.84	0.90	0.57	0.55

Table 5
FMA Spatial std deviation (°N/S).

Region	El Niño	Neutral	La Niña	Climate
Africa	4.71	5.16	5.18	5.62
Indian	2.67	3.18	3.35	4.08
Australia	1.29	3.24	2.90	2.01
WPacific	1.15	3.37	2.93	1.99
CPacific	2.26	3.10	3.23	2.27
EPacific	1.48	1.74	2.33	4.80
SAmerica	3.37	5.61	2.72	3.39
Atlantic	0.88	0.32	0.92	1.04

northern ITCZ during the DJF and JFM seasons (Figs. 2 and 4 (b and c)). Chen et al. (2021) can be consulted for more details on the drivers of the collapsing double-ITCZ to a more equatorial ITCZ during the extreme El Niño years.

To quantify the spatial variability of the ITCZ over different regions we calculated the standard deviation based on the zonal mean of the ITCZ for the region. This provides the average degree North/South (N/S) variability of the ITCZ over the region.

Tables 2–5 show the region specific spatial standard (std) deviation of the ITCZ for the extreme El Niño and extreme La Niña in comparison to the neutral ENSO and climatological position for NDJ (Table 2), DJF (Table 3), JFM (Table 4), and FMA (Table 5) during the Austral summer seasons.

The seasonal spatial variability of the ITCZ position for the climate period is lowest over the Atlantic Ocean for all Austral summer seasons. The spatial variability is highest over Africa for all seasons during extreme La Niña and neutral (except for FMA season) phases of ENSO.

3.3. Relationship between interannual ITCZ variability, average ITCZ, and average SSTs during El Niño, La Niña, and neutral phases of Austral summer seasons

The African ITCZ and ONI cross-wavelet and coherence analysis are applied to investigate their association over Africa. The analysis is also used to identify the possible existence of the physical (dynamic) link between these two drivers of global precipitation variability, an African case study.

Based on Fig. 7(a–c), there is a clear SSTs (28 °C contour to the south of the Equator around the central to eastern Pacific) distinction between the three phases of ENSO during NDJ and the position of the ITCZ is found within the warmer SSTs. The ITCZ position during the NDJ season shows a higher La Niña spatial variation than the El Niño (Fig. 7e). This is most evident over Africa ($\sigma =$ 4.84 and 3.99 during La Niña and El Niño, respectively), the Indian Ocean, Australia, WPacific Ocean, EPacific Ocean ($\sigma = 0.92$ and 0.65 during La Niña and El Niño, respectively), and the Atlantic Ocean. Alternatively, over the CPacific Ocean, and SAmerica ($\sigma = 5.21$ and 4.91 during El Niño and La Niña, respectively), the El Niño years manifest a higher spatial variability than the La Niña years. The climatological position of the ITCZ reflects a more pronounced spatial variability than both the El Niño and the La Niña phases (Fig. 7e)

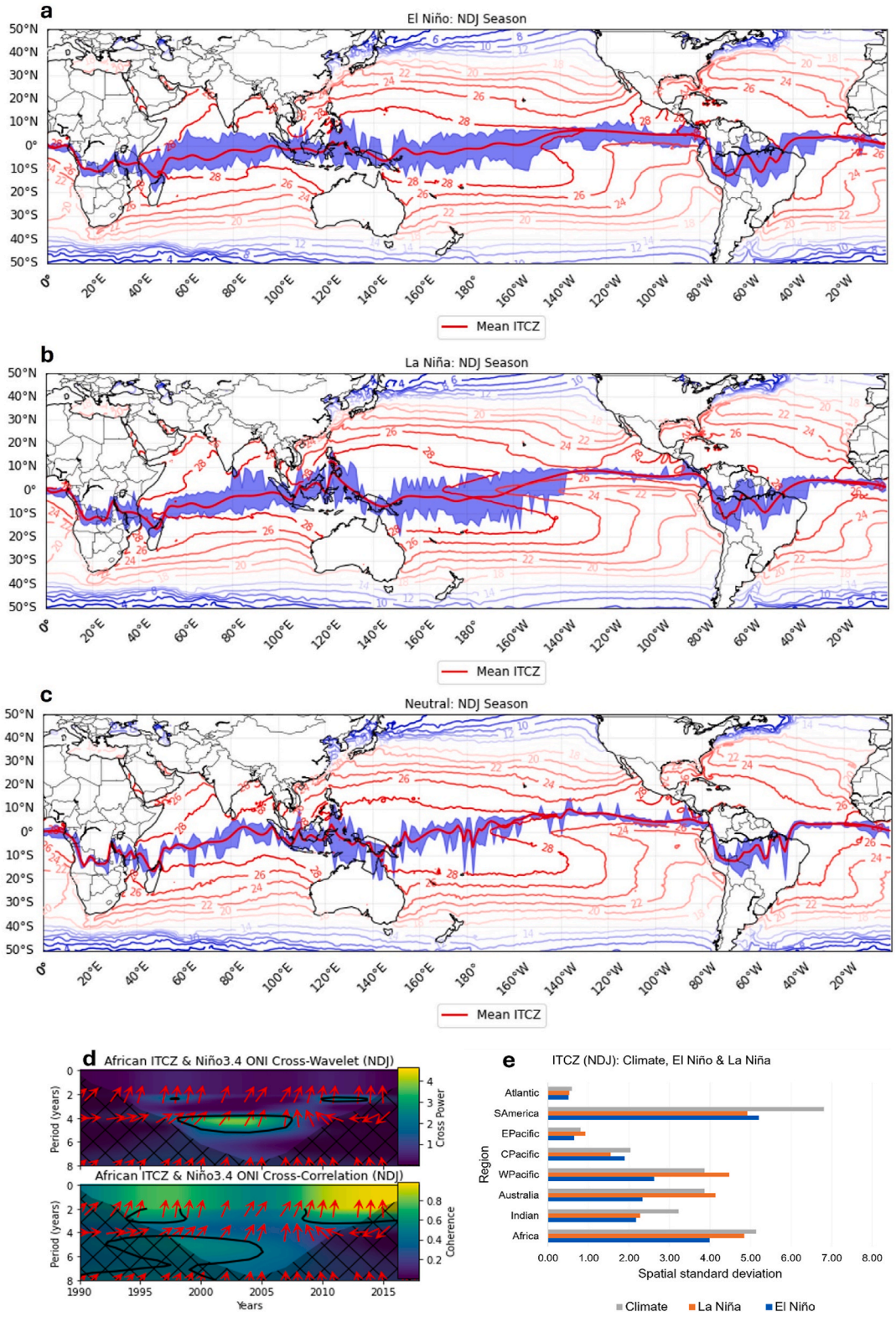

(caption on next page)

Fig. 7. The mean position of the ITCZ (red line) for NDJ, its year-on-year variability (blue plume), and related seasonal mean SSTs (contours) during the El Niño (a), La Niña (b), and neutral (c) phases. The cross-wavelet power and wavelet cross-correlation analysis between the Niño 3.4 ONI and African ITCZ for the NDJ season is presented by (d). The thick black contour designates the 5 % significance level against red noise and the edge effects are demarcated by the mesh. The relative phase relationship is portrayed by arrows with in phase pointing right-up, antiphase pointing down, while right or left arrows reflect the phase lag between ONI and ITCZ position. The regional north-south variability of the ITCZ is represented by spatial standard deviation (e). (For interpretation of the references to colour in this figure legend, the reader is referred to the Web version of this article.)

during the NDJ season for Africa, Indian Ocean, CPacific, SAmerica and Atlantic Ocean. Over Africa, the signal from the Niño 3.4 is expected to have physical effects that are linked to key rain bearing aspects of the climate system because ENSO plays a vital role in southern African rainfall variability (Gillett et al., 2023; Lenssen et al., 2020; Monerie et al., 2019). The variations are spatially well reflected in Figs. 2e, 3(e) and 4(e). The cross-wavelet analysis between the ONI and the NDJ African ITCZ is shown in Fig. 7d. This is meant to extract possible covariation between the ONI and the NDJ African ITCZ by exposing regions of high common power and the phase of the covariation. The figure shows a four-year periodicity at a relatively high common power. The two are also in phase with correlation coefficients of 0.4 and above. However, it should be noted that the correlations are not reflected as statistically significant, potentially because the variability of the ITCZ position could be explained by other drivers other than the ENSO signal alone.

According to Fig. 8e, the DJF ITCZ position shows a higher year-on-year La Niña spatial variation than the year-on-year El Niño spatial variation over Africa, the Indian Ocean, Australia, WPacific Ocean, CPacific Ocean, and the EPacific Ocean. This shows an extension of spatial variability, over the Pacific Ocean, from what it was during the NDJ season. Over SAmerica to Atlantic Ocean, the year-on-year El Niño ($\sigma = 5.25/0.59$ for SAmerica/Atlantic respectively) shows a higher variability than the year-on-year La Niña ($\sigma = 4.96/0.49$ for SAmerica/Atlantic respectively) phase. The climatological ITCZ shows a higher spatial variability than both El Niño and La Niña throughout all the regions except the Central and Eastern Pacific Oceans where La Niña shows the highest variability. Over the Atlantic Ocean, the highest variability between climatology, El Niño and La Niña phases is found during the El Niño. These variations are well reflected in Figs. 2e, 3e and 4e where their year-on-year variation plume has been used. Once again there is a clear distinction of the warmest SSTs (especially the 28 °C contour south of the Equator, on the central to eastern Pacific Ocean) between the ENSO phases during DJF as reflected by Fig. 8(a–c). The location of the maximum precipitation is also within the warmer SSTs. The DJF distribution of the SSTs, Fig. 8(a–c), is similarly found in Keshtgar et al. (2020) even though they used the ERA-Interim dataset. Similarly, the zonal ITCZ position over the Indian ocean (represented by 60°E − 100°E in this study) during DJF season is 5.5°S which is comparable to the 5.5°S annual position over the Indian Ocean (represented by 40°E − 110°E) found in Keshtgar et al. (2020). The cross-wavelet power analysis between the DJF ONI and the DJF African ITCZ (Fig. 8, d) shows that there are common features between the two-time series such as a significant peak with four-year period over 1995–2013 time band. Compared with the power spectrum from NDJ, DJF shows an increased power for the two series. The ONI and the ITCZ are also in phase with correlation coefficients of 0.6 and above, a better correlation than observed in NDJ. It is important to note the much lower power in the series can be seen for NDJ compared to DJF. However, the area of significant correlation is so extensive that it is unlikely that the similarity in the shared power of the signals is simply by chance.

According to Fig. 9(a–c), there is a dissipation of the clarity in warmer SSTs (28 °C contour to the south of the Equator on the central to the eastern Pacific Ocean) distinction between the three phases of ENSO during JFM. Similarly, the spatial standard deviation over all regions for El Niño and La Niña are comparable. This indicates that the distinction between both phases is beginning to disappear. However, the ITCZ position during JFM season still shows a higher year-on-year variation during La Niña than the variation during El Niño over Africa, the Indian Ocean, Australia, WPacific Ocean, CPacific Ocean, and EPacific Ocean. Furthermore, the variability has again extended further eastward, from what it covered in DJF season, to include SAmerica as well. During this season, it's only over the Atlantic Ocean where the year-on-year El Niño shows a higher variability than the year-on-year La Niña. The climatological spatial variability persists to be the highest between the El Niño and La Niña phases except over the Atlantic Ocean where the variability is highest during El Niño.

The covariance analysis between the JFM ONI and the JFM African ITCZ (Fig. 9d) shows an even higher cross power over a four-year periodicity than the DJF power spectrum. The JFM coherence levels are also stronger ($\geq$0.7) than the DJF coherence levels. However, the significance of these coherence levels is lower than the significance observed for DJF. Both the ONI and African ITCZ in JFM are strongly correlated, with a consistent and slow varying phase lag. The high coherence, phase lag, and low significance levels between the two signals suggest that the two time-series are physically linked but such physical link must be subject to influence by other factors which require further studies beyond the scope of this paper.

In terms of the areas under which the spatial variability is higher during La Niña than it is during El Niño, FMA has similar coverage as the DJF season, further reflection of the retreating spatial variability. This is also seen with the SSTs distribution in which all three phases have nearly the same SST distribution. The other outstanding feature observed during FMA season is how the El Niño ITCZ position occurs to the north of the climatology position over the Indian Ocean for all the El Niño years in this study (Fig. 10a). Figs. 2e, 3(e) and 4(e), provide details of the year-on-year spatial variation of the ITCZ during El Niño, neutral and La Niña phases of ENSO where it can easily be picked from the plume distribution that the La Niña year-on-year ITCZ variation is higher than the El Niño year-on-year variation over Africa, the Indian Ocean, Australia, WPacific Ocean, CPacific Ocean, and the EPacific Ocean.

The FMA cross-wavelet power analysis between the ONI and the African ITCZ (Fig. 10d) shows lower statistical significance levels for oscillations in ITCZ that manifest in the common 4-year periodicity. The ONI and ITCZ are still in phase with a cross-correlation coefficient of 0.5 and above. The fact that there is slowly varying time-lag across all time scales suggests that there are multiple physical mechanisms of signal propagation at play in influencing the fluctuation of the ITCZ across the seasons and years. The

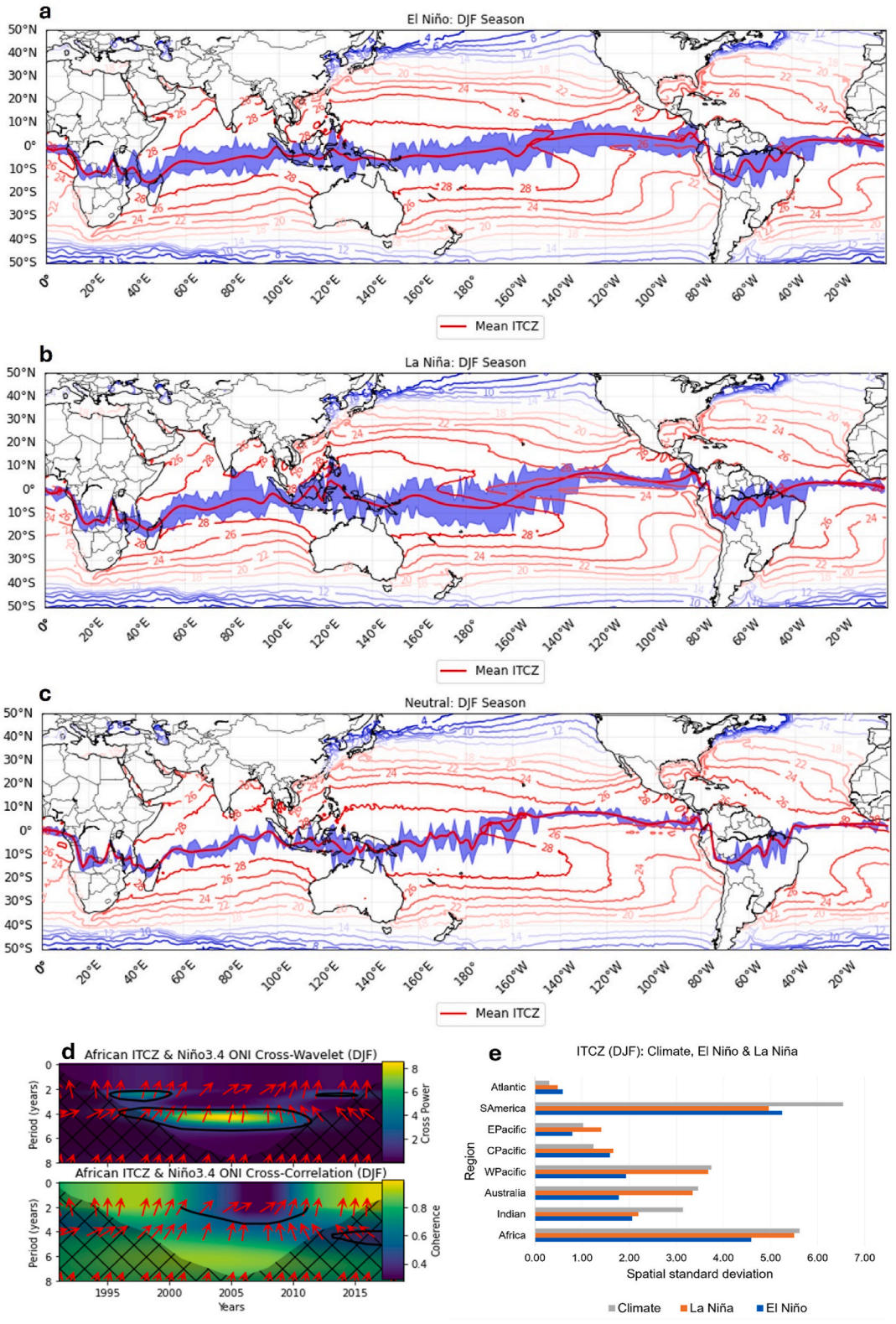

(caption on next page)

Fig. 8. The DJF mean position of the ITCZ (red line), its year-on-year variability (blue plume), and corresponding SSTs (contours) during the El Niño (a), La Niña (b), and neutral (c) phases. The cross-wavelet power and wavelet cross-correlation analysis between the Niño 3.4 ONI and African ITCZ for the DJF season is presented by (d) and the regional north-south variability of the ITCZ is represented by spatial (e). (For interpretation of the references to colour in this figure legend, the reader is referred to the Web version of this article.)

deviation from in-phase to slow time lag is evident across the significant power time band. This is suggestive that ITCZ position can change slightly leading to lagging behind the ONI. A detailed analysis of the standard deviation between the distribution of the two signals (Tables 2–5) during the positive and negative phases of the ENSO extremes ranked from 4.07 to 5.67 solidify the conclusion that there are additional processes or drivers whose temporal behavior cannot be explained by looking at the variability of ONI alone.

The regional rain bearing system drivers such as the South Indian Ocean Dipole (SIOD) are some of the internal variability candidate processes that could be explored to establish how teleconnections contribute to the distribution of the high intensity precipitation areas over the African tropics. While this study has, as its focus, an understanding of the link between the ENSO and ITCZ positional shifts, the influence of external forcing such as radiative forcing/asymmetric heating responsible for the temperature gradients between land and sea, Southern and Northern Hemisphere cannot be overlooked.

The highest amount of precipitation occurs within the warmest SSTs (Figs. 7–10). This is aligned to the finding by Zhang et al. (2021) in their study which covered the annual zonal mean position of the global ITCZ using the Global Precipitation Climatology Project (GPCP) monthly mean precipitation from 1981 to 2010. Furthermore, the results from this study suggest that the global position of the ITCZ is closely related to the ocean currents: it shifts northward while approaching the cold currents and shifts (back) southward after passing the cold current or while approaching the warm current. Overall, these seasonal migration and variability of the global ITCZ are consistent with the results from Roldán-Gómez et al. (2022) even though they applied the centroid method to determine the ITCZ position. The observed jump of the ITCZ in the pacific ocean around 160°W/E is related to the double ITCZ where there are two areas on both sides of the equator receiving high precipitation (Gonzalez et al., 2022; Yan and Li, 2018; Zhang et al., 2021). The climatological position of the ITCZ shows higher spatial variability than the position during the El Niño/La Niña throughout all the regions except over parts of the Pacific Ocean during El Niño/La Niña phases of the ENSO. This shows a certain level of co-variability between Pacific Ocean's ITCZ and the ENSO phases.

The higher spatial standard deviations and higher year-on-year variability in the ENSO-based ITCZ position reflects the uniqueness of each El Niño/La Niña event. The same observation, on the uniqueness of each El Niño/La Niña year, has been thoroughly reported on by Chen et al. (2021) who focused on the differences that exists within each individual El Niño year using the three (1982/83, 1997/98 & 2015/16) extreme El Niño years. The current study and that of Chen et al. (2021) uncover aspects of ITCZ variability that point to the need for a detailed analysis of the various drivers of the rain bearing systems and their teleconnection in the light of the ITCZ spatial shifts across the seasons.

The ITCZ position over the Eastern Pacific and Atlantic Oceans consistently, from NDJ to FMA seasons, shows (Figs. 7–10 (e)) minimal spatial variation as compared to all other regions for climatological, El Niño, and La Niña ITCZ. According to Jiang et al. (2021), the Atlantic Ocean ITCZ is found to be very narrow wherein the ENSO impacts on Atlantic ITCZ reflect a signature of modulation by the local seasonal precipitation cycle. This is evidenced by the Atlantic Ocean experiencing the lowest σ through most of the seasons and the three ENSO phases (Figs. 7–10 (e)). Similar to Windmiller and Stevens (2023), the Atlantic ITCZ shows only a slight change along the longitude during July and August. Table 7 in Appendix a reflects the narrowness (based on the difference between climatology and neutral as well as the difference between extreme El Niño and extreme La Niña) of the position of the Atlantic ITCZ variability ranges.

Based on Figs. 7–10, the African and Atlantic ITCZ show a lower year-on-year variability (as reflected by the plume) throughout all the Austral summer seasons while the SAmerican ITCZ only shows lower spatial variation in JFM and FMA. The high spatial variability (symbolized by higher σ) over SAmerica is a result of around 13.99° shift of the ITCZ position within a 2.5° change in longitudes along the SAmerican Westcoast (283.75–286.25°E). On the other hand, the high spatial variability over Africa (symbolized by higher spatial σ) is a result of around 6.14° shift of the ITCZ position within a 2.5° change in longitudes along the African Westcoast (13.75–16.25°E). A combination of these massive shifts and minimal year-on-year variation as reflected by the plume leads to the conclusion that both SAmerican and African ITCZ have low year-on-year climatological, El Niño, and La Niña ITCZ variation. The spatial standard deviation over Atlantic Ocean and the observed minimal year-on-year variation (plume) are aligned, and both show lower spatial variability. Similarly, Suzuki (2011) concluded that the African (10°–40°E) ITCZ is robust and simple mechanisms drive its seasonal migration. Suzuki used ERA-40 dataset in their study. The magnitude of seasonal variation of the ITCZ in response to ENSO phases is found to be lowest over the Atlantic Ocean and EPacific. The magnitude of seasonal variation of the ITCZ over Africa, and SAmerica is also regarded minimal if we put context to the changes over their West coast and in consideration of the year-on-year variability (plume).

The possibility of the position of the ITCZ being a secondary response to the teleconnection mechanisms that affect Global Climate is interesting and worth exploring. A comprehensive investigation of the teleconnections could help establish causal connections between the response of the ITCZ to individual El Niño/La Niña year. Most of the previous studies make selective choice of certain teleconnection indices to study physical effects that are deemed relevant, for example, the Indian Ocean Dipole (IOD) influences the

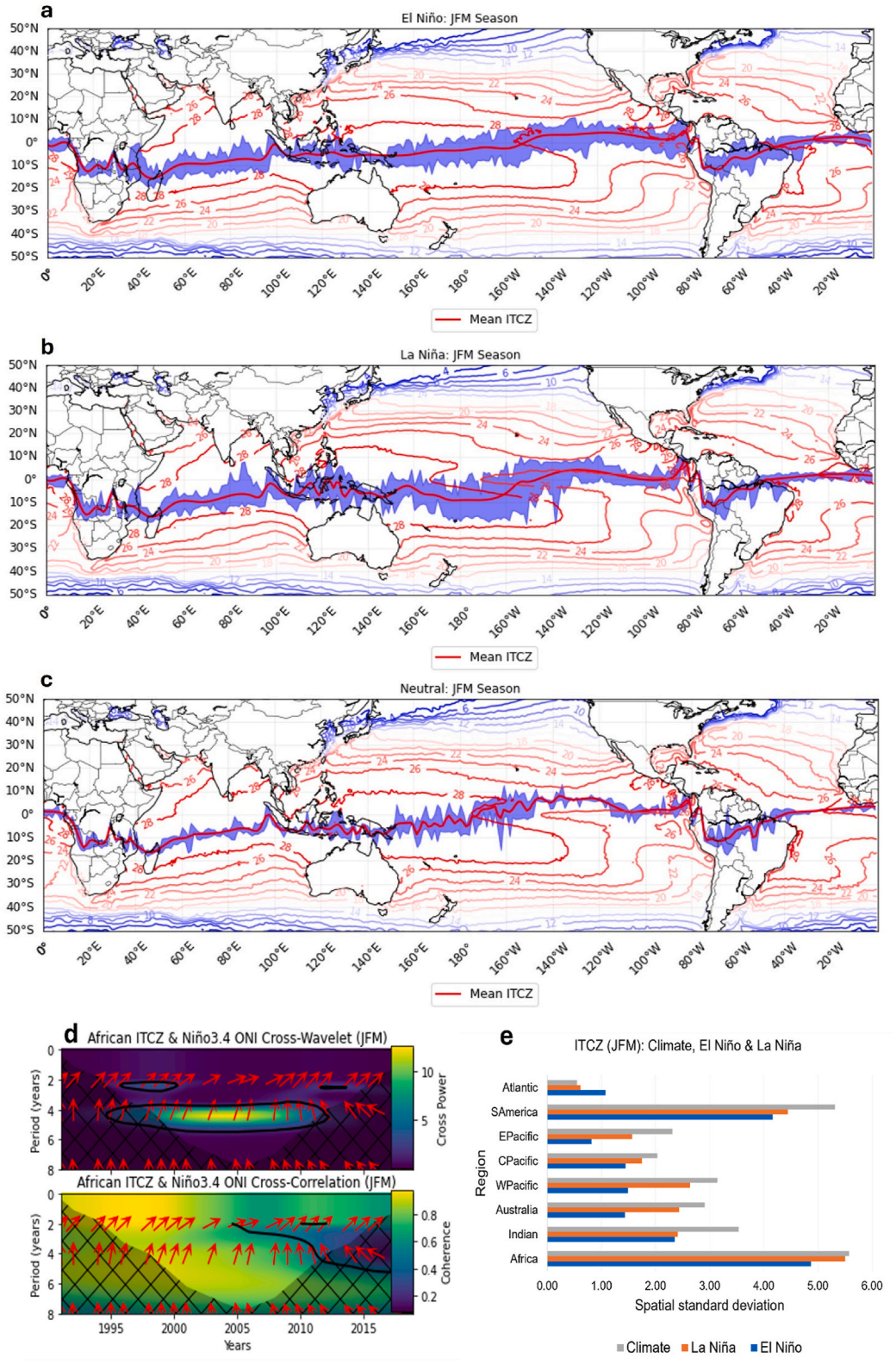

(caption on next page)

Fig. 9. The JFM mean position of the ITCZ (red line), its year-on-year variability (blue plume), and corresponding SSTs (contours) during the El Niño (a), La Niña (b), and neutral (c) phases. The cross-wavelet power and wavelet cross correlation analysis between the Niño 3.4 ONI and African ITCZ for the JFM seasons is presented by (d) and the regional north-south variability is represented by spatial standard deviation (e). (For interpretation of the references to colour in this figure legend, the reader is referred to the Web version of this article.)

southern African October–December rainfall variability (Ogwang et al., 2020) and it has been well established by Reason (2001) that southern African rainfall is influenced by the South Indian Ocean subtropical SSTs dipole. Furthermore, the Indian Ocean ITCZ is influenced by the South Indian Ocean Dipole (SIOD) that is independent of the ENSO phases; what is generally referred to be Pure Positive SIOD (P_PSIOD) and Pure Negative SIOD (P_NSIOD) by Dong et al. (2023). The study concludes that combination of ENSO and SIOD interactions leads to a different response of the ITCZ for any given El Niño/La Niña year. The general impression on the analysis and other related studies (De Albuquerque Cavalcanti, 2015; Yang et al., 2018) that explore the effects of a few isolated potential drivers of the ITCZ position, across the globe, is an emergent phenomena driven by complex, multi-dimensional and potentially interacting mechanism of signal propagation.

4. Conclusion

This study explored the spatial and seasonal response of the global ITCZ position to the different ENSO phases (including their extremes) during the Austral summer seasons between November (current year) and April (the following year). By comparing the alignment between the position of the ITCZ determined from the maximum precipitation to the surface tropical wind convergence using ERA5 re-analysis dataset, commonalities and divergence between these patterns are established. There is an alignment between the ITCZ position determined from the maximum precipitation index and the surface tropical wind convergence, especially over the oceanic areas. However, there are some identified differences between the ITCZ position as determined by maximum precipitation and the surface tropical wind convergence over the central to western Pacific Ocean during all the three phases of ENSO and all seasons. This misalignment is possibly the result of the double ITCZ (Chen et al., 2008; Samanta et al., 2019). It is, however, noticed that the plume covers the entire area between the north-easterly and south-easterly winds over these areas. There is no alignment between the precipitation-based and surface tropical wind convergence-based ITCZ over the continents. This is possibly a result of the topographic effects on convergence areas, over the continents, amongst many other factors.

The study on global and regional exploration of the spatio-temporal variability of the ITCZ response to different extreme ENSO phases found that there is consistency in the behavior of the zonal position of the global and regional ITCZ which is detectable across the different parameters. Over Africa, there is a noticeable South Ward shift in the position of ITCZ moving from long term average position to long term La Niña position to extreme La Niña position. A similar shift, but in the opposite direction, is found in the case of extreme El Niño, particularly during the early to late summer seasons. We hypothetically conclude that there must be some well-defined physical mechanisms that link ENSO, and its extremes to the ITCZ position over Africa based on the African ITCZ's consistency in response. Despite Australia being in the Southern Hemisphere, the Australian ITCZ response to ENSO and its extremes relative to the long-term position is strongly delineated from its neighborhood. This indicates that ENSO and its extremes are not as strongly linked to the position of the Australian ITCZ as they are to the African and South American ITCZ.

The cross-wavelet and coherence analysis show that over Africa, the ITCZ position and the ONI time series have common features in the wavelet power such as a significant peak of high power in 4-year period band indicating that the evolution of the ITCZ position completely mirror that of the ONI every 4 years. However, the phase lag between the signals leads to the conclusion that other mechanisms are linked to the shift in position at variable strength and direction over time. Furthermore, the wavelet analysis of the ONI from 1950 to 2022 provides a maximum of 0.6 °C variance in the 2–8 year scale-averaged power. This indicates the minor differences that exists, in intensity, between the El Niño/La Niña events. However, such minor intensity differences drive major precipitation distribution differences. Therefore, this suggests that there should be other mechanisms influencing the regional precipitation over and above the well-defined response to the ENSO phases. The mechanisms that influence the location of maximum seasonal precipitation can be extracted through teleconnections studies between ENSO and regional rain-bearing systems which is beyond the scope of the current research.

The teleconnection studies between the ITCZ shifts and drivers of internal variability open an opportunity for improved interpretation of seasonal forecasts of hydroclimatic events. Under climate change conditions, this could set the basis for anticipation of the response of precipitation, at various regions of the globe, to internally driven fluctuations in the dominant atmospheric and ocean states.

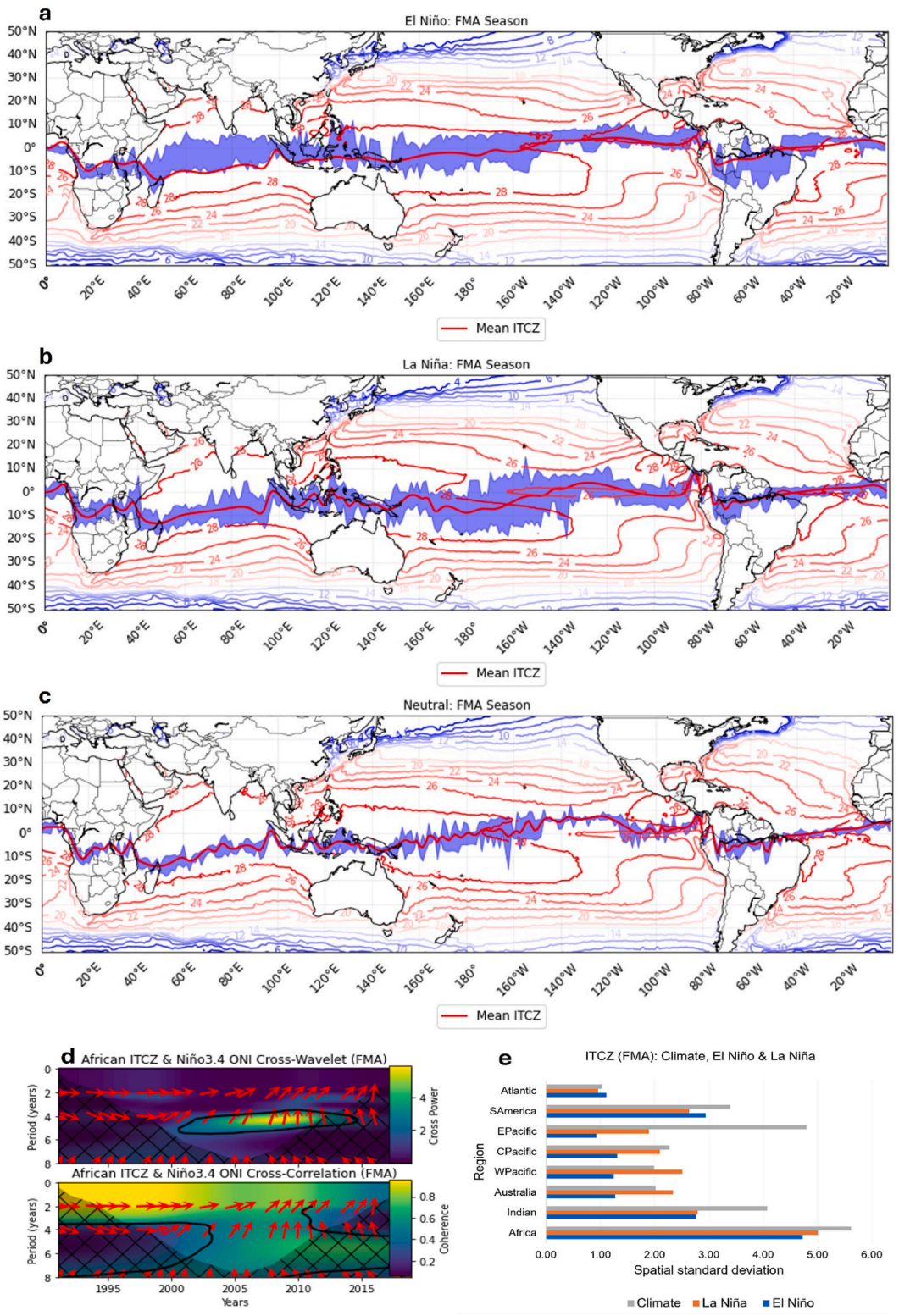

Fig. 10. The FMA mean position of the ITCZ (red line), its year-on-year variability (blue plume), and related SSTs (contours) during the El Niño (a), La Niña (b), and neutral (c) phases. The cross-wavelet power and wavelet cross-correlation analysis between the Niño 3.4 ONI and African ITCZ for the FMA seasons is presented by (d) and the regional north-south variability is represented by spatial standard deviation (e). (For interpretation of the references to colour in this figure legend, the reader is referred to the Web version of this article.)

CRediT authorship contribution statement

Teke S. Ramotubei: Writing – review & editing, Writing – original draft, Visualization, Validation, Software, Methodology, Investigation, Formal analysis, Conceptualization. **Willem A. Landman:** Writing – review & editing, Visualization, Supervision, Conceptualization. **Mohau J. Mateyisi:** Writing – review & editing, Visualization, Supervision. **Shingirai S. Nangombe:** Writing – review & editing, Visualization, Supervision. **Asmerom F. Beraki:** Writing – review & editing, Visualization, Supervision.

Data availability statement

The European Centre for Medium-Range Weather Forecasts (ECMWF) fifth generation reanalysis (ERA5) at 0.25° * 0.25° resolution (Hersbach et al., 2020) is utilized in this study and can be accessed from ERA5 monthly averaged data on single levels from 1940 to present (copernicus.eu) while Oceanic Niño Index (ONI) data used is based on three month running mean of sea surface temperature (SST) anomalies in the Niño 3.4 region as obtained from the Extended Reconstructed Sea Surface Temperature version5 (ERSSTv5) (Huang et al., 2017) and can be accessed via Climate Prediction Center - ONI (noaa.gov).

Declaration of competing interest

The authors declare the following financial interests/personal relationships which may be considered as potential competing interests:Teke Solomon Ramotubei reports financial support, administrative support, and article publishing charges were provided by Council for Scientific and Industrial Research. If there are other authors, they declare that they have no known competing financial interests or personal relationships that could have appeared to influence the work reported in this paper.

Acknowledgements

This work was supported by the Department of Science and Innovation parliamentary grant (P1FCM00) received by the Climate and Air Quality Modelling group of the Council for Scientific and Industrial Research and the FOCUS-AFRICA project, which has received funding from the European H2020 Research and Innovation program (Grant Agreement 869575).

Appendix A

Table 6
Zonal Position of the ITCZ (in °N) comparison between the climatological position, the mean of the extreme three El Niño years, and the mean of the extreme three La Niña years.

Zonal ITCZ position (Climate, 3 extreme El Niño years & 3 extreme La Niña) in °N												
Region	NDJ			DJF			JFM			FMA		
	Climate	El Niño	La Niña	Climate	El Niño	La Niña	Climate	El Niño	La Niña	Climate	El Niño	Nina
Africa	−7.53	−5.61	−8.15	−9.05	−7.88	−10.08	−9.01	−8.52	−9.88	−7.05	−6.94	−7.5
Indian	−3.43	−1.66	−1.82	−5.5	−5.3	−3.77	−7.24	−7.59	−6.75	−6.96	−8.42	−6.4
Australia	−2.54	−2.49	−1.84	−4.58	−5.15	−4.63	−5.38	−5.39	−5.55	−4.58	−5.17	−4.86
WPacific	−2.57	−2.53	−1.17	−4.63	−5.27	−4.15	−5.55	−5.37	−5.26	−4.66	−5.06	−5.25
CPacific	0.37	−2.53	−1.17	−5.2	−5.27	−4.15	−9.6	−5.37	−5.26	−4.64	−5.06	−5.25
EPacific	7.25	4.91	7.7	6.43	2.9	5.3	4.45	1.29	2.07	4.29	1.12	0.71
SAmerica	−5.42	−5.32	−2.87	−6.48	−7.69	−3.82	−5.28	−6.7	−3.92	−3.19	−2.96	−2.54
Atlantic	4.08	3.08	3.95	3.03	1.95	2.77	2.5	1.03	1.77	2.61	2.2	0.91

Table 7
Differences between the mean of the three extreme El Niño years and mean of the three extreme La Niña years through the Austral summer seasons and differences between Climatology (1991–2020) & the three Neutral ENSO years through all the Austral summer seasons.

Region explored	NDJ		DJF		JFM		FMA		Nov–Apr mean	
	Clim-Neutral	Niño - Niña	Clim-Neutral	Niño - Niña	Clim-Neutral	Niño - Niña	Clim-Neutral	Niño - Niña	Clim-Neutral	Niño - Niña
Africa	0.02	2.54	−0.09	2.19	0.02	1.37	−0.37	0.56	−0.105	1.665
Indian	−1.34	0.16	−0.37	−1.53	−0.68	−0.85	−0.77	−2.02	−0.79	−1.06
Australia	1.07	−0.65	1.45	−0.52	0.68	0.16	0.43	−0.31	0.9075	−0.33
WPacific	1.4	−1.35	1.84	−1.12	0.86	−0.11	0.46	0.19	1.14	−0.5975
CPacific	−0.72	−0.32	−3.68	2.65	−7.75	3.22	−3.81	3.44	−3.99	2.2475
EPacific	0.2	−2.79	−0.08	−2.4	−0.48	−0.78	−0.3	0.41	−0.165	−1.39
SAmerica	0.15	−2.45	0.18	−3.87	0.18	−2.77	0.13	−0.42	0.16	−2.3775
Atlantic	0.47	−0.87	0.36	−0.82	0.54	−0.74	1.27	1.29	0.66	−0.285

Appendix B. Variability of the ITCZ for different regions during NDJ seasons. Comparing the climate to the extreme El Niño/La Niña positions

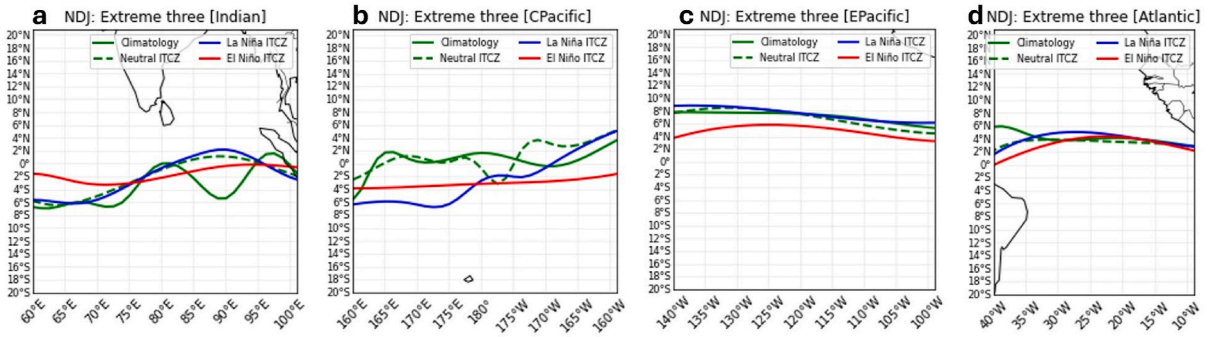

Appendix C. Variability of the ITCZ for different regions during DJF seasons. Comparing the climate to the extreme El Niño/La Niña positions

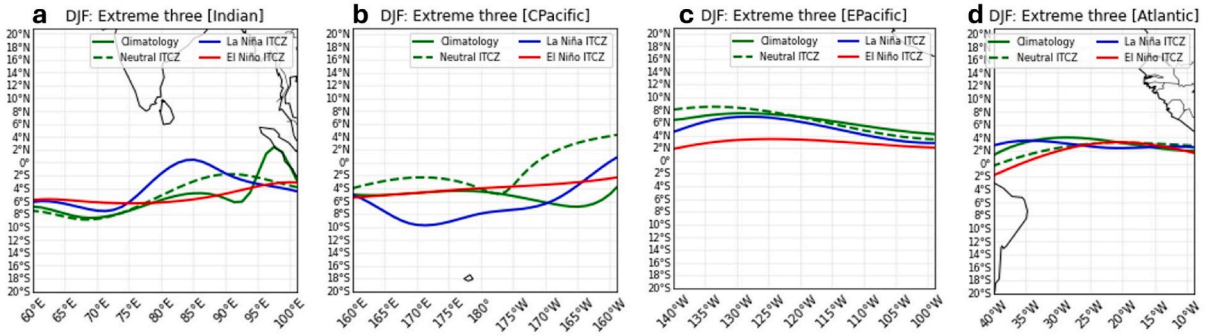

Appendix D. Variability of the ITCZ for different regions during JFM seasons. Comparing the climate to the extreme El Niño/La Niña positions

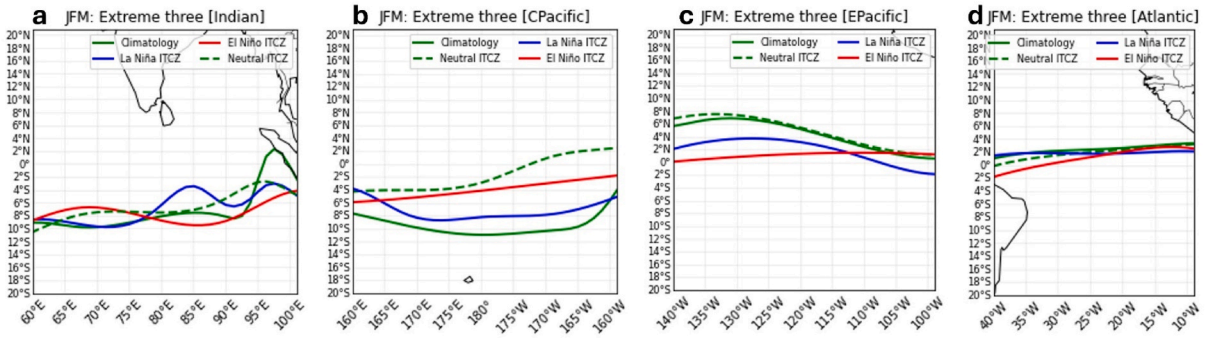

Appendix E. Variability of the ITCZ for different regions during FMA seasons. Comparing the climate to the extreme El Niño/La Niña positions

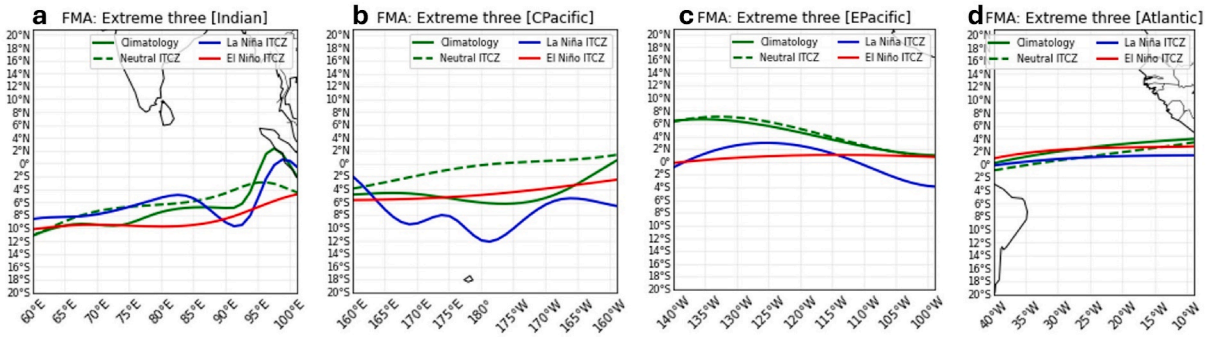

Appendix F. Zonal position of the ITCZ during the three extreme La Niña years and three extreme El Niño years against the climatological position over different regions

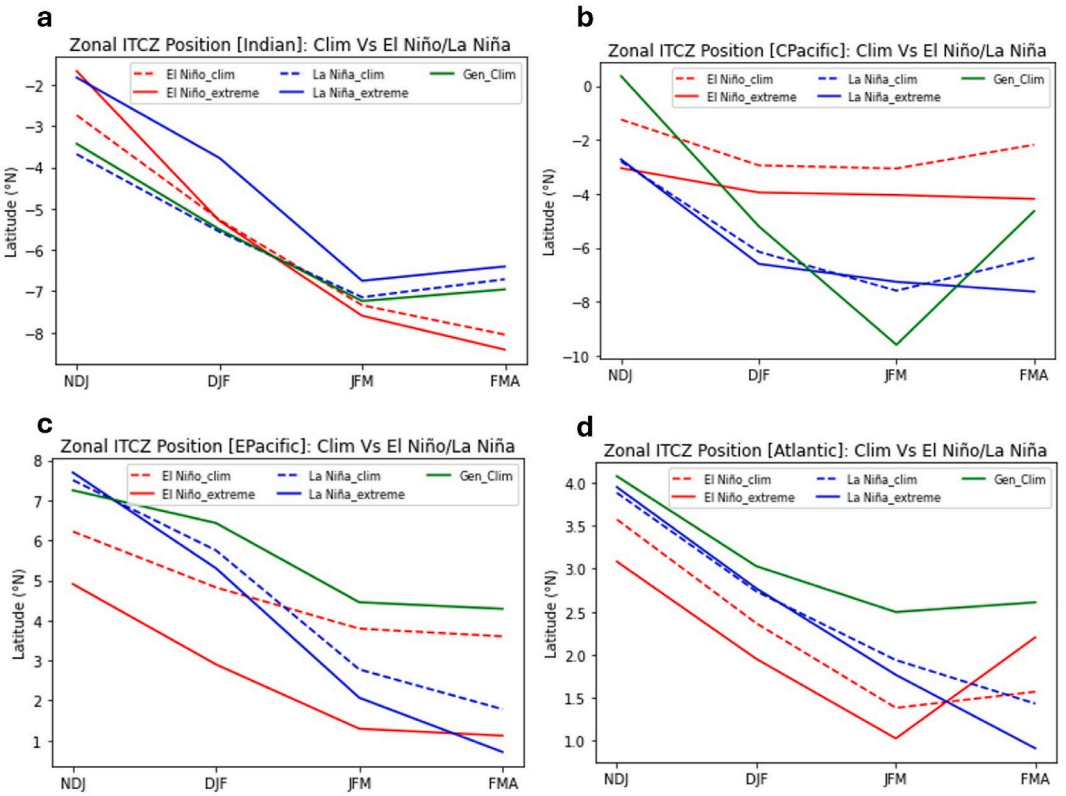

Appendix G. : Climatology of global ITCZ based on maximum precipitation and minimum divergence (Min_Div) for NDJ, DJF, JFM, and FMA

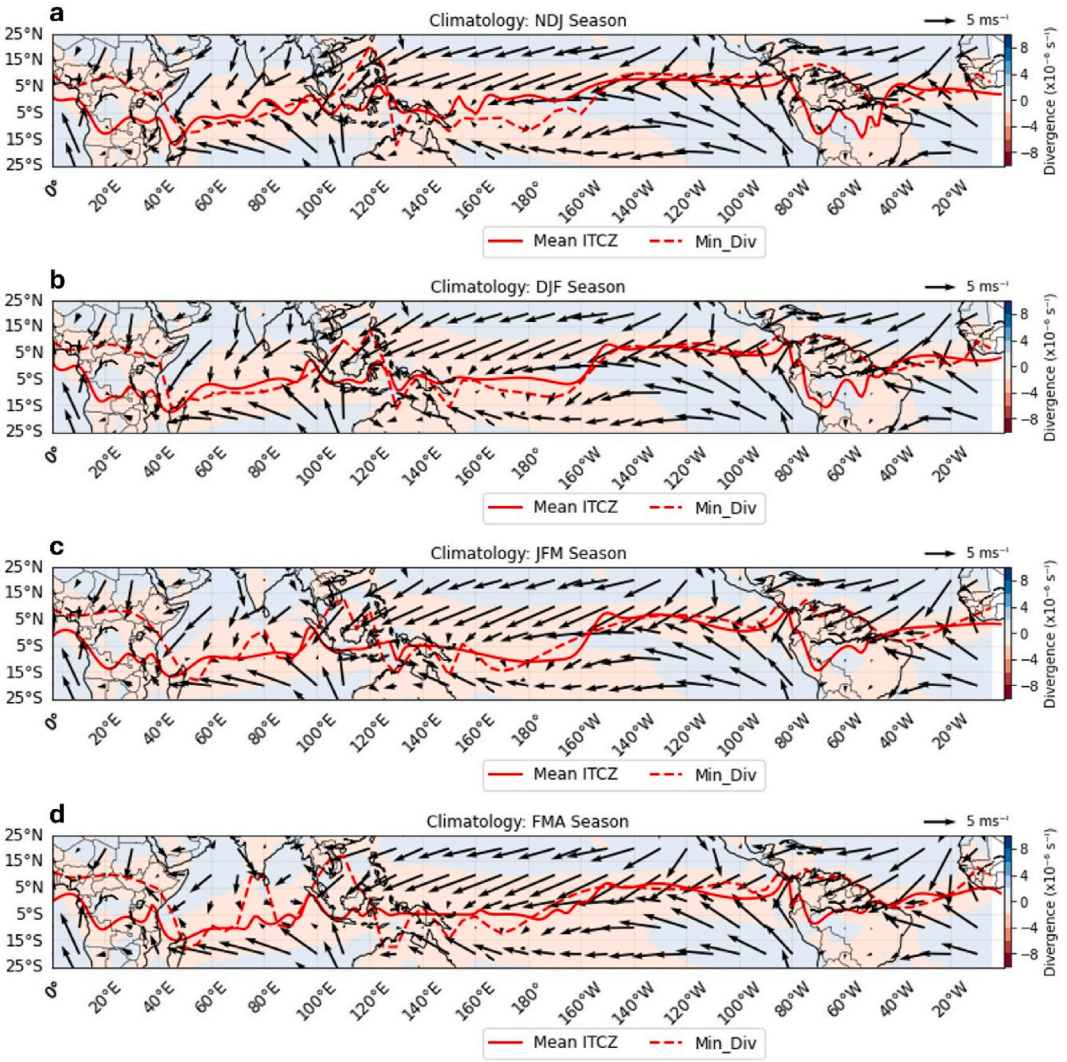

Data availability

Data will be made available on request.

References

Adam, O., Bischoff, T., Schneider, T., 2016. Seasonal and interannual variations of the energy flux equator and ITCZ. Part II: zonally varying shifts of the ITCZ. J. Clim. 29 (20), 7281–7293. https://doi.org/10.1175/JCLI-D-15-0710.1.

Arguez, A., Vose, R.S., 2011. The definition of the standard WMO climate normal: the key to deriving alternative climate normals. Bull. Am. Meteorol. Soc. 92 (6), 699–704.

Burns, S.J., McGee, D., Scroxton, N., Kinsley, C.W., Godfrey, L.R., Faina, P., Ranivoharimanana, L., 2022. Southern Hemisphere controls on ITCZ variability in southwest Madagascar over the past 117,000 years. Quat. Sci. Rev. 276, 107317. https://doi.org/10.1016/j.quascirev.2021.107317.

Chen, B., Lin, X., Bacmeister, J.T., 2008. Frequency distribution of daily ITCZ patterns over the western–central pacific. J. Clim. 21 (17), 4207–4222. https://doi.org/10.1175/2008JCLI1973.1.

Chen, Y., Yan, L., Li, G., Xu, J., Long, J., Zheng, S., 2021. Contrasting impacts of three extreme El niños on double ITCZs over the eastern Pacific Ocean. Atmosphere 12 (4), 424. https://doi.org/10.3390/atmos12040424.

De Albuquerque Cavalcanti, I.F., 2015. The influence of extratropical Atlantic Ocean region on wet and dry years in North-Northeastern Brazil. Front. Environ. Sci. 3. https://doi.org/10.3389/fenvs.2015.00034.
Dong, R., Guan, Y., Zhou, W., Guo, C., 2023. Impact of Southern Indian ocean dipole via the ITCZ on winter and spring precipitation in China. Atmos. Ocean. Sci. Let. 16 (6), 100358. https://doi.org/10.1016/j.aosl.2023.100358.
Faulk, S., Mitchell, J., Bordoni, S., 2017. Effects of rotation rate and seasonal forcing on the ITCZ extent in planetary atmospheres. J. Atmos. Sci. 74 (3), 665–678. https://doi.org/10.1175/JAS-D-16-0014.1.
Frierson, D.M.W., Hwang, Y.-T., 2012. Extratropical influence on ITCZ shifts in slab ocean simulations of global warming. J. Clim. 25 (2), 720–733. https://doi.org/10.1175/JCLI-D-11-00116.1.
Gbode, I.E., Babalola, T.E., Diro, G.T., Intsiful, J.D., 2023. Assessment of ERA5 and ERA-interim in reproducing mean and extreme climates over west Africa. Adv. Atmos. Sci. 40 (4), 570–586. https://doi.org/10.1007/s00376-022-2161-8.
Gillett, Z.E., Taschetto, A.S., Holgate, C.M., Santoso, A., 2023. Linking ENSO to synoptic weather systems in eastern Australia. Geophys. Res. Lett. 50 (15), e2023GL104814. https://doi.org/10.1029/2023GL104814.
Gleixner, S., Demissie, T., Diro, G.T., 2020. Did ERA5 improve temperature and precipitation reanalysis over east Africa? Atmosphere 11 (9), 996. https://doi.org/10.3390/atmos11090996.
Gonzalez, A.O., Ganguly, I., McGraw, M.C., Larson, J.G., 2022. Rapid dynamical evolution of ITCZ events over the east Pacific. J. Clim. 35 (4), 1197–1213. https://doi.org/10.1175/JCLI-D-21-0216.1.
Grodsky, S.A., 2003. Near surface westerly wind jet in the Atlantic ITCZ. Geophys. Res. Lett. 30 (19), 2009. https://doi.org/10.1029/2003GL017867.
Hersbach, H., Bell, B., Berrisford, P., Hirahara, S., Horányi, A., Muñoz-Sabater, J., Nicolas, J., Peubey, C., Radu, R., Schepers, D., Simmons, A., Soci, C., Abdalla, S., Abellan, X., Balsamo, G., Bechtold, P., Biavati, G., Bidlot, J., Bonavita, M., et al., 2020. The ERA5 global reanalysis. Q. J. R. Meteorol. Soc. 146 (730), 1999–2049. https://doi.org/10.1002/qj.3803.
Horton, P., 2022. Analogue methods and ERA5: benefits and pitfalls. Int. J. Climatol. 42 (7), 4078–4096. https://doi.org/10.1002/joc.7484.
Huang, B., Thorne, P.W., Banzon, V.F., Boyer, T., Chepurin, G., Lawrimore, J.H., Menne, M.J., Smith, T.M., Vose, R.S., Zhang, H.-M., 2017. Extended reconstructed Sea Surface temperature, version 5 (ERSSTv5): upgrades, validations, and intercomparisons. J. Clim. 30 (20), 8179–8205. https://doi.org/10.1175/JCLI-D-16-0836.1.
Jiang, F., Zhang, W., Jin, F., Stuecker, M.F., 2021. Meridional migration of ENSO impact on tropical atlantic precipitation controlled by the seasonal cycle. Geophys. Res. Lett. 48 (24), e2021GL096365. https://doi.org/10.1029/2021GL096365.
Keshtgar, B., Alizadeh-Choobari, O., Irannejad, P., 2020. Seasonal and interannual variations of the intertropical convergence zone over the Indian Ocean based on an energetic perspective. Clim. Dyn. 54 (7–8), 3627–3639. https://doi.org/10.1007/s00382-020-05195-5.
Lashkari, H., Mohammadi, Z., Keikhosravi, G., 2017. Annual fluctuations and displacements of inter tropical convergence zone (ITCZ) within the range of Atlantic Ocean-India. Open J. Ecol. 7 (1), 12–33. https://doi.org/10.4236/oje.2017.71002.
Lau, W.K.M., Kim, K.-M., Chern, J.-D., Tao, W.K., Leung, L.R., 2020. Structural changes and variability of the ITCZ induced by radiation–cloud–convection–circulation interactions: inferences from the Goddard Multi-scale Modeling Framework (GMMF) experiments. Clim. Dyn. 54 (1–2), 211–229. https://doi.org/10.1007/s00382-019-05000-y.
Lenssen, N.J.L., Goddard, L., Mason, S., 2020. Seasonal forecast skill of ENSO teleconnection maps. Weather Forecast. 35 (6), 2387–2406. https://doi.org/10.1175/WAF-D-19-0235.1.
Liu, C., Liao, X., Qiu, J., Yang, Y., Feng, X., Allan, R.P., Cao, N., Long, J., Xu, J., 2020. Observed variability of intertropical convergence zone over 1998—2018. Environ. Res. Lett. 15 (10), 104011. https://doi.org/10.1088/1748-9326/aba033.
Marshall, J., Donohoe, A., Ferreira, D., McGee, D., 2014. The ocean's role in setting the mean position of the Inter-Tropical Convergence Zone. Clim. Dyn. 42 (7–8), 1967–1979. https://doi.org/10.1007/s00382-013-1767-z.
May, R.M., Goebbert, K.H., Thielen, J.E., Leeman, J.R., Camron, M.D., Bruick, Z., Bruning, E.C., Manser, R.P., Arms, S.C., Marsh, P.T., 2022. MetPy: a meteorological Python library for data analysis and visualization. Bull. Am. Meteorol. Soc. 103 (10), E2273–E2284. https://doi.org/10.1175/BAMS-D-21-0125.1.
Mischell, E., Lee, J.-E., 2022. Observed zonal variations of the relationship between ITCZ position and meridional temperature contrast. Climate 10 (3), 30. https://doi.org/10.3390/cli10030030.
Monerie, P.-A., Robson, J., Dong, B., Dieppois, B., Pohl, B., Dunstone, N., 2019. Predicting the seasonal evolution of southern African summer precipitation in the DePreSys3 prediction system. Clim. Dyn. 52 (11), 6491–6510. https://doi.org/10.1007/s00382-018-4526-3.
Morales-Velázquez, M.I., Herrera, G.D.S., Aparicio, J., Rafieeinasab, A., Lobato-Sánchez, R., 2021. Evaluating reanalysis and satellite-based precipitation at regional scale: a case study in southern Mexico. Atmósfera. https://doi.org/10.20937/ATM.52789.
Mosaffa, H., Filippucci, P., Massari, C., Ciabatta, L., Brocca, L., 2023. SM2RAIN-Climate, a monthly global long-term rainfall dataset for climatological studies. Sci. Data 10 (1), 749. https://doi.org/10.1038/s41597-023-02654-6.
Navidi Nassaj, B., Zohrabi, N., Nikbakht Shahbazi, A., Fathian, H., 2022. Evaluating the performance of eight global gridded precipitation datasets across Iran. Dynam. Atmos. Oceans 98, 101297. https://doi.org/10.1016/j.dynatmoce.2022.101297.
Nicholson, S.E., 2018. The ITCZ and the seasonal cycle over equatorial Africa. Bull. Am. Meteorol. Soc. 99 (2), 337–348. https://doi.org/10.1175/BAMS-D-16-0287.1.
Ogwang, B.A., Ongoma, V., Shilenje, Z.W., Ramotubei, T.S., Letuma, M., Ngaina, J.N., 2020. Influence of Indian Ocean dipole on rainfall variability and extremes over southern Africa. Mausam 71 (4), 637–648. https://doi.org/10.54302/mausam.v71i4.50.
Philander, S.G.H., Gu, D., Lambert, G., Li, T., Halpern, D., Lau, N.-C., Pacanowski, R.C., 1996. Why the ITCZ is mostly north of the Equator.pdf. J. Clim. 9 (12), 2958–2972. https://doi.org/10.1175/1520-0442(1996)009<2958:WTIIMN>2.0.CO;2.
Quagraine, K.A., Nkrumah, F., Klein, C., Klutse, N.A.B., Quagraine, K.T., 2020. West African summer monsoon precipitation variability as represented by reanalysis datasets. Climate 8 (10), 111. https://doi.org/10.3390/cli8100111.
Randriatsara, H.H.-R.H., Hu, Z., Ayugi, B., Makula, E.K., Vuguziga, F., Nkunzimana, A., 2022. Interannual characteristics of rainfall over Madagascar and its relationship with the Indian Ocean sea surface temperature variation. Theor. Appl. Climatol. https://doi.org/10.1007/s00704-022-03950-8.
Reason, C.J.C., 2001. Subtropical Indian Ocean SST dipole events and southern African rainfall. Geophys. Res. Lett. 28 (11), 2225–2227. https://doi.org/10.1029/2000GL012735.
Roldán-Gómez, P.J., González-Rouco, J.F., Melo-Aguilar, C., Smerdon, J.E., 2022. The role of internal variability in ITCZ changes over the last millennium. Geophys. Res. Lett. 49 (4), e2021GL096487. https://doi.org/10.1029/2021GL096487.
Samanta, D., Karnauskas, K.B., Goodkin, N.F., 2019. Tropical pacific SST and ITCZ biases in climate models: double trouble for future rainfall projections? Geophys. Res. Lett. 46 (4), 2242–2252. https://doi.org/10.1029/2018GL081363.
Shen, Z., Yong, B., Gourley, J.J., Qi, W., Lu, D., Liu, J., Ren, L., Hong, Y., Zhang, J., 2020. Recent global performance of the climate Hazards group infrared precipitation (CHIRP) with Stations (CHIRPS). J. Hydrol. 591, 125284. https://doi.org/10.1016/j.jhydrol.2020.125284.
Silva, E.H.D.L., Silva, F.D.D.S., Junior, R.S.D.S., Pinto, D.D.C., Costa, R.L., Gomes, H.B., Júnior, J.B.C., De Freitas, I.G.F., Herdies, D.L., 2022. Performance assessment of different precipitation databases (gridded analyses and reanalyses) for the new Brazilian agricultural frontier: SEALBA. Water 14 (9), 1473. https://doi.org/10.3390/w14091473.
Steinkopf, J., Engelbrecht, F., 2022. Verification of ERA5 and ERA-Interim precipitation over Africa at intra-annual and interannual timescales. Atmos. Res. 280, 106427. https://doi.org/10.1016/j.atmosres.2022.106427.
Suzuki, T., 2011. Seasonal variation of the ITCZ and its characteristics over central Africa. Theor. Appl. Climatol. 103 (1–2), 39–60. https://doi.org/10.1007/s00704-010-0276-9.
Tadeyo, E., Chen, D., Ayugi, B., Yao, C., 2020. Characterization of spatio-temporal trends and periodicity of precipitation over Malawi during 1979–2015. Atmosphere 11 (9), 891. https://doi.org/10.3390/atmos11090891.
Torrence, C., Compo, G.P., 1998. A practical guide to wavelet analysis. Bull. Am. Meteorol. Soc. 79 (1), 61–78. https://doi.org/10.1175/1520-0477(1998)079<0061:APGTWA>2.0.CO;2.

Torrence, C., Webster, P.J., 1999. Interdecadal changes in the ENSO–monsoon system. J. Clim. 12 (8), 2679–2690. https://doi.org/10.1175/1520-0442(1999)012<2679:ICITEM>2.0.CO;2.

Vindel, J.M., Valenzuela, R.X., Navarro, A.A., Polo, J., 2020. Temporal and spatial variability analysis of the solar radiation in a region affected by the intertropical convergence zone. Meteorol. Appl. 27 (1), e1824. https://doi.org/10.1002/met.1824.

Waliser, D.E., Gautier, C., 1993. A satellite-derived climatology of the ITCZ. J. Clim. 6 (11), 2162–2174. https://doi.org/10.1175/1520-0442(1993)006<2162:ASDCOT>2.0.CO;2.

Wei, H., Bordoni, S., 2020. Energetic constraints on the intertropical convergence zone position in the observed seasonal cycle from modern-era retrospective analysis for research and applications, version 2 (MERRA-2). Geophys. Res. Lett. 47 (16). https://doi.org/10.1029/2020GL088506.

Windmiller, J.M., Stevens, B., 2023. The inner life of the Atlantic ITCZ. Q. J. R. Meteorol. Soc. 4610. https://doi.org/10.1002/qj.4610 qj.

Wolf, F., Voigt, A., Donner, R.V., 2020. A climate network perspective of the intertropical convergence zone [Preprint]. Dynam. Earth Sys.: Inter. https://doi.org/10.5194/esd-2020-81.

Wu, X., Liang, X.-Z., Zhang, G.J., 2003. Seasonal migration of ITCZ precipitation across the equator: why can't GCMs simulate it? Geophys. Res. Lett. 30 (15). https://doi.org/10.1029/2003GL017198.

Yan, L., Li, G., 2018. Double intertropical convergence zones over the eastern Pacific Ocean: contrasting impacts of the eastern Pacific- and central Pacific-type El Niños. Atmos. Sci. Lett. 19 (10), e852. https://doi.org/10.1002/asl.852.

Yang, S., Li, Z., Yu, J.-Y., Hu, X., Dong, W., He, S., 2018. El niño–southern oscillation and its impact in the changing climate. Natl. Sci. Rev. 5 (6), 840–857. https://doi.org/10.1093/nsr/nwy046.

Zhang, H., Ma, X., Zhao, S., Kong, L., 2021. Advances in research on the ITCZ: mean position, model bias, and anthropogenic aerosol influences. J. Meteorol. Res. 35 (5), 729–742. https://doi.org/10.1007/s13351-021-0203-2.

Zhu, J., Liu, Y., Xie, R., Chang, H., 2018. A comparative analysis of the impacts of two types of El Niño on the central and eastern pacific ITCZ. Atmosphere 9 (7), 266. https://doi.org/10.3390/atmos9070266.